Supplementary Information

Mortality risk from heat-stress expected to hit poorest nations the hardest

Ali Ahmadalipour[1*], Hamid Moradkhani[1], Mukesh Kumar[1]

[1]*Center for Complex Hydrosystems Research, Department of Civil, Construction, and Environmental Engineering, University of Alabama, Tuscaloosa, AL 35487*

*Corresponding author: aahmada@ua.edu

Table of Contents

1. Material and Methods

1.1. Climate Data

Table S1. The 17 RCMs used in this study and their characteristics. All the RCMs have a spatial resolution of 0.44° and they are analyzed at a daily temporal resolution.

No	Deriving GCM	Original Modeling Institute	Original Resolution (lat x lon)	Domain	Ens. Member	Downscaling Institute*	Tx	hurs
1	CanESM2	Canadian Centre for Climate Modeling and Analysis	2.8° × 2.8°	AFR-44	r1i1p1	SMHI	✓	✓
2	CNRM-CM5	National Centre of Meteorological Research, France	1.4° × 1.4°	AFR-44	r1i1p1	CLM	✓	×
3				AFR-44		SMHI	✓	✓
4				MNA-44		SMHI	✓	✓
5	CSIRO-Mk3-6-0	Commonwealth Scientific and Industrial Research Organization, Australia	1.8° × 1.8°	AFR-44	r1i1p1	SMHI	✓	✓
6	EC-EARTH	EC-EARTH consortium	1.0° × 1.0°	AFR-44	r12i1p1	CLM	✓	×
7				AFR-44	r12i1p1	MPI	✓	×
8				AFR-44	r12i1p1	SMHI	✓	✓
9				MNA-44	r12i1p1	SMHI	✓	✓
10	GFDL-ESM2M	Geophysical Fluid Dynamics Laboratory	2.5° × 2.0°	AFR-44	r1i1p1	SMHI	✓	✓
11				MNA-44	r1i1p1	SMHI	✓	✓
12	IPSL-CM5A-MR	Institut Pierre-Simon Laplace	2.5° × 1.25°	AFR-44	r1i1p1	SMHI	✓	✓
13	MIROC5	Atmosphere and Ocean Research Institute (The University of Tokyo), National Institute for Environmental Studies, and Japan Agency for Marine-Earth Science and Technology	1.4° × 1.4°	AFR-44	r1i1p1	SMHI	✓	✓
14	MPI-ESM-LR	Max Planck Institute for Meteorology (MPI-M)	1.9° × 1.9°	AFR-44	r1i1p1	CLM	✓	×
15					r1i1p1	MPI	✓	×
16					r1i1p1	SMHI	✓	✓
17	NorESM1-M	Norwegian Climate Centre	2.5° × 1.9°	AFR-44	r1i1p1	SMHI	✓	✓

*SMHI: Swedish Meteorological and Hydrological Institute; CLM: Climate Limited-area Modelling Community;

1.2. Calculating wet-bulb temperature (TW)

Wet-bulb temperature (TW) provides a proxy for the real-feel temperature and a measure for human discomfort, which is more reliable for health risk assessments (Pal and Eltahir 2016; Coffel et al. 2017; Im et al. 2018). Wet-bulb temperature is calculated at a daily timescale using the maximum near-surface air temperature and relative humidity as follows (Stull 2011):

$$TW = Tx \times \operatorname{atan}\left[0.151977(RH\% + 8.313659)^{\frac{1}{2}}\right] + \operatorname{atan}(Tx + RH\%) -$$

$$\operatorname{atan}(RH\% - 1.676331) + 0.00391838(RH\%)^{\frac{3}{2}}\operatorname{atan}(0.023101RH\%) - 4.686035 \qquad (1)$$

where Tx is the maximum near surface air temperature (in °C), *RH%* is the relative humidity, and *TW* is the wet-bulb temperature in Celsius. Although more complex methods have been implemented for calculating TW (Pal and Eltahir 2016), the equation used in this study has proven to be accurate for a wide range of relative humidity (5%-99%) and for temperatures as high as 50°C (Stull 2011), thus making it applicable to the Middle East and North Africa (MENA). TW is calculated using Equation 1 at a daily timescale for each RCM, and is later used to obtain the optimum temperature and quantify mortality risk.

1.3. Quantifying mortality risk

Quantification of mortality risk is performed using a recently developed empirical function derived based on global epidemiological studies analyzing the impacts of excess temperature on all-cause mortality of people aged over 65 years old, including the external causes such as deaths from heatstroke and heat-related accidents (Honda et al. 2014; WHO 2014). It has been demonstrated that heat-related mortality reaches the lowest value at an optimum temperature (T_{opt}), and increases subsequently with rise in temperature beyond T_{opt}. The 84th percentile of maximum daily temperature has been found to closely capture the postulated T_{opt} across over 90% of the cities

worldwide (Honda et al. 2014; Ahmadalipour and Moradkhani 2018). Therefore, here we set T_{opt} for each grid in each model to be equal to the 84th percentile of historical daily TW. The spatially explicit threshold allows accounting for regional physiological attributes of human body and its tolerance to heat. The calculated T_{opt} of each RCM is shown in Figure 1.

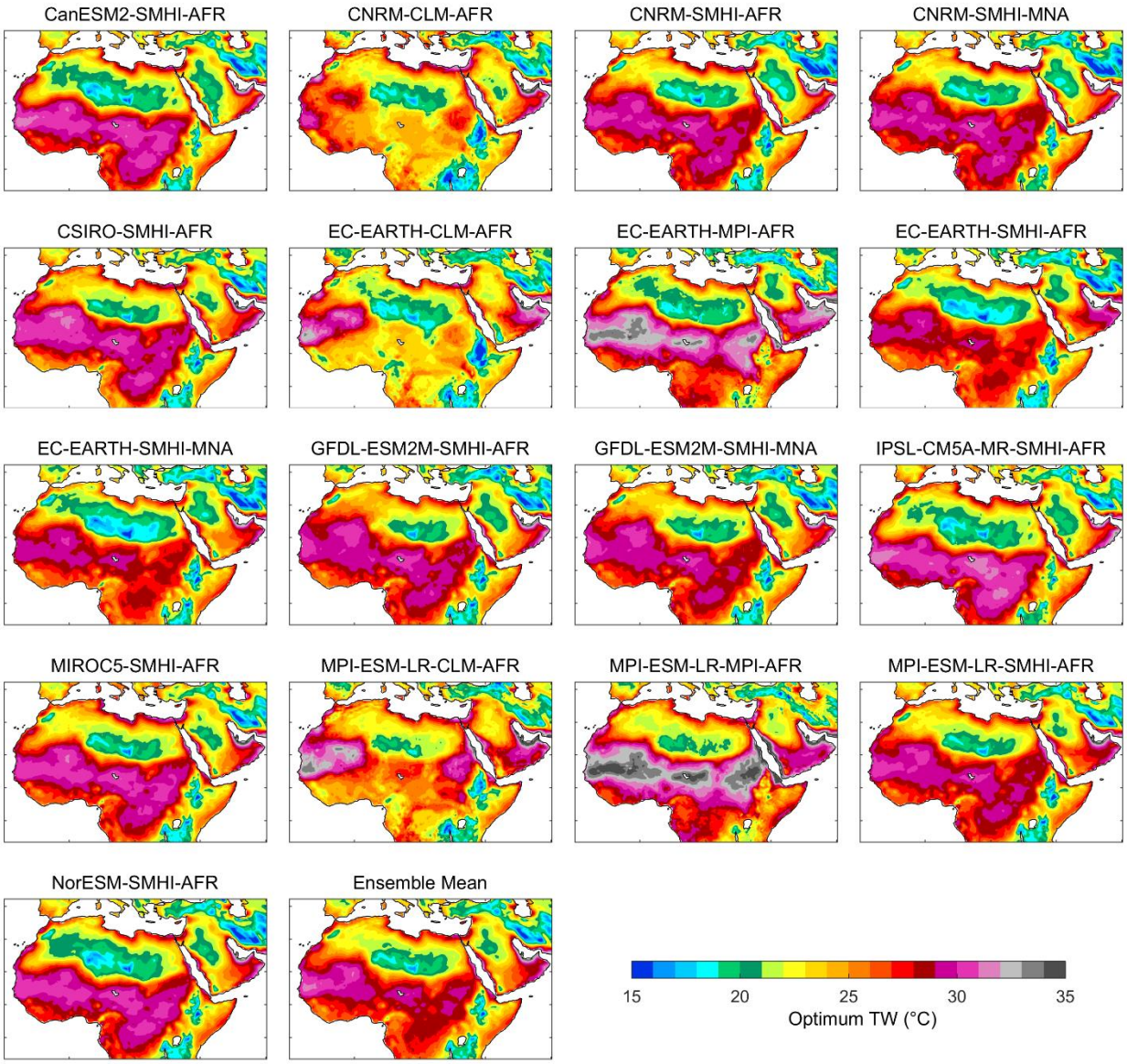

Figure S1. Optimum wet-bulb temperature (Topt) calculated for each RCM and the ensemble mean (last plot) using the historical data for the period of 1951-2005.

The daily relative mortality risk (RMR) is calculated based on the temperature offset ($\Delta T = TW - T_{opt}$) using the following equation (Honda et al. 2014; WHO 2014; Ahmadalipour and Moradkhani 2018):

$$RMR = -2.91 \times 10^{-5} \Delta T^3 + 0.00153 \Delta T^2 + 0.0054 \Delta T + 1 \quad (2)$$

For temperatures below T_{opt}, RMR=1. Therefore, in order to obtain the excess mortality risk, RMR-1 is calculated for each day. The daily RMR is then accumulated for the entire summer to calculate summer excess mortality risk as follows:

$$Summer\ Excess\ Mortality\ Risk = \sum_{n=1}^{N} (RMR_n - 1) \quad (3)$$

where N indicates the number of unsafe days (days with $TW > T_{opt}$ yielding RMR>1) in a particular year. The methodology to quantify mortality risk is presented in Figure 2. The calculated summer excess mortality risk of each year in two future pathways are compared to the long-term historical mean summer mortality risk to obtain the mortality risk ratio (MRR). MRR represents the change in mortality risk with respect to the historical period.

$$(Mortality\ Risk\ Ratio)_i|_{i=2006:2100} = \frac{(Summer\ Excess\ Mortality\ Risk)_i}{Historical\ Mean\ Summer\ Mortality\ Risk} \quad (4)$$

In order to assess the long-term impacts of climate change, the mean MRR is calculated for near future period (2010-2039), an intermediate future period (2040-2069), and a distant future period (2070-2099) for each RCM in each future concentration pathways.

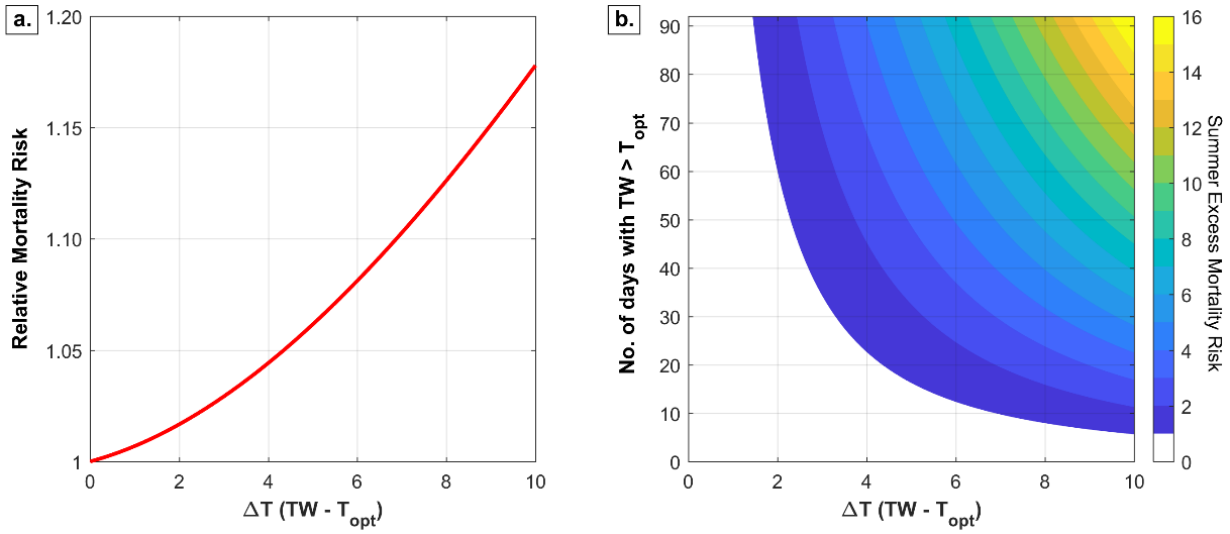

Figure S2. a) The function used to quantify the relative mortality risk based on temperature offset. b) Summer excess mortality risk as a function of temperature offset and frequency.

2. Climate change analysis

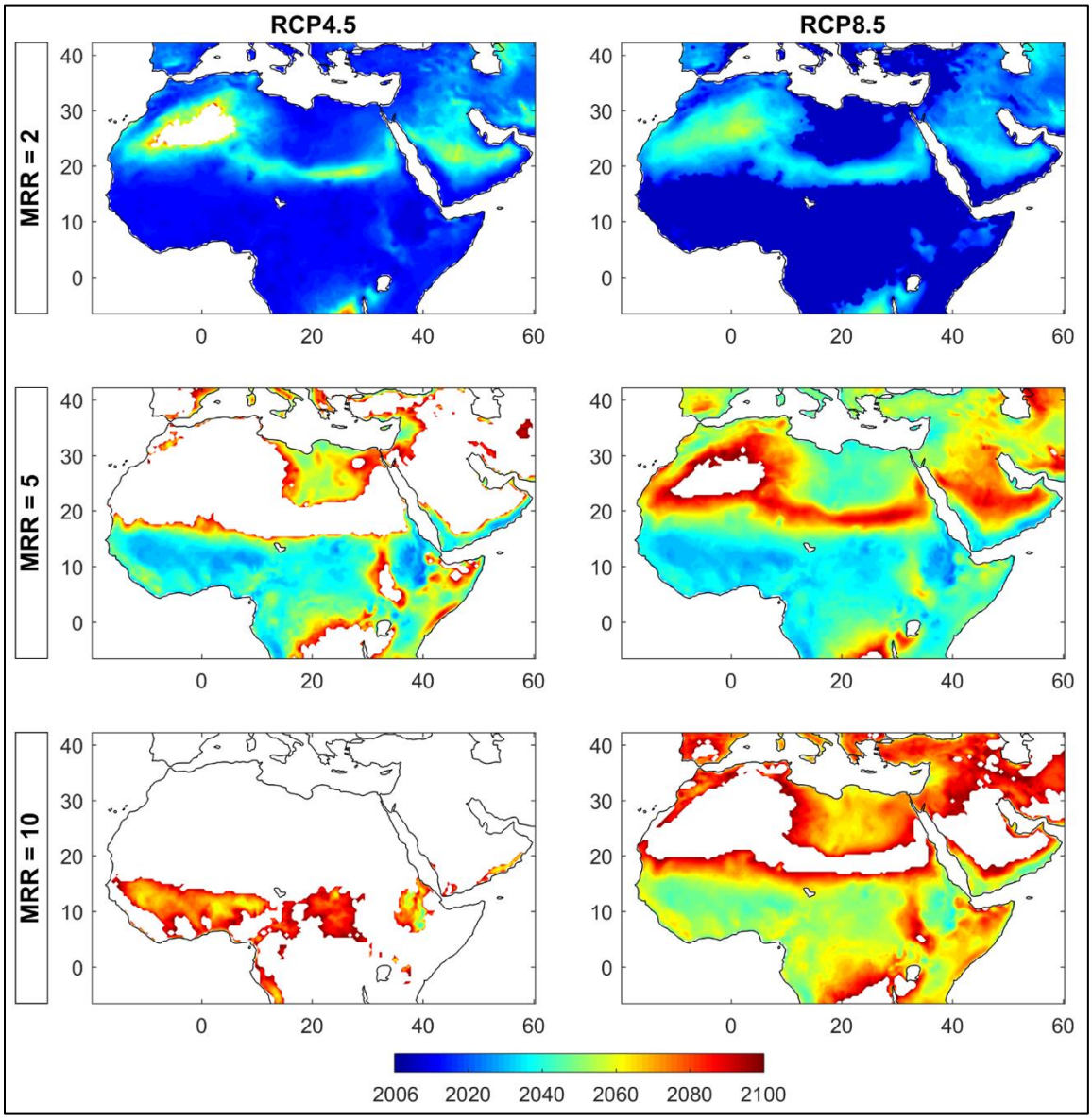

Figure S3. Time of emergence for mortality risk ratio (MRR) to become 2-fold (top row), 5-fold (middle row), and 10-fold (bottom row) compared to the historical mortality risk. The figure is generated using the results of ensemble mean of 17 RCMs. Areas with no data imply that the MRR will not reach the specified level within the period. The figure indicates that the mortality risk has already doubled in central Africa and it will become 5-fold within the next 10-15 years (sometime around 2030s).

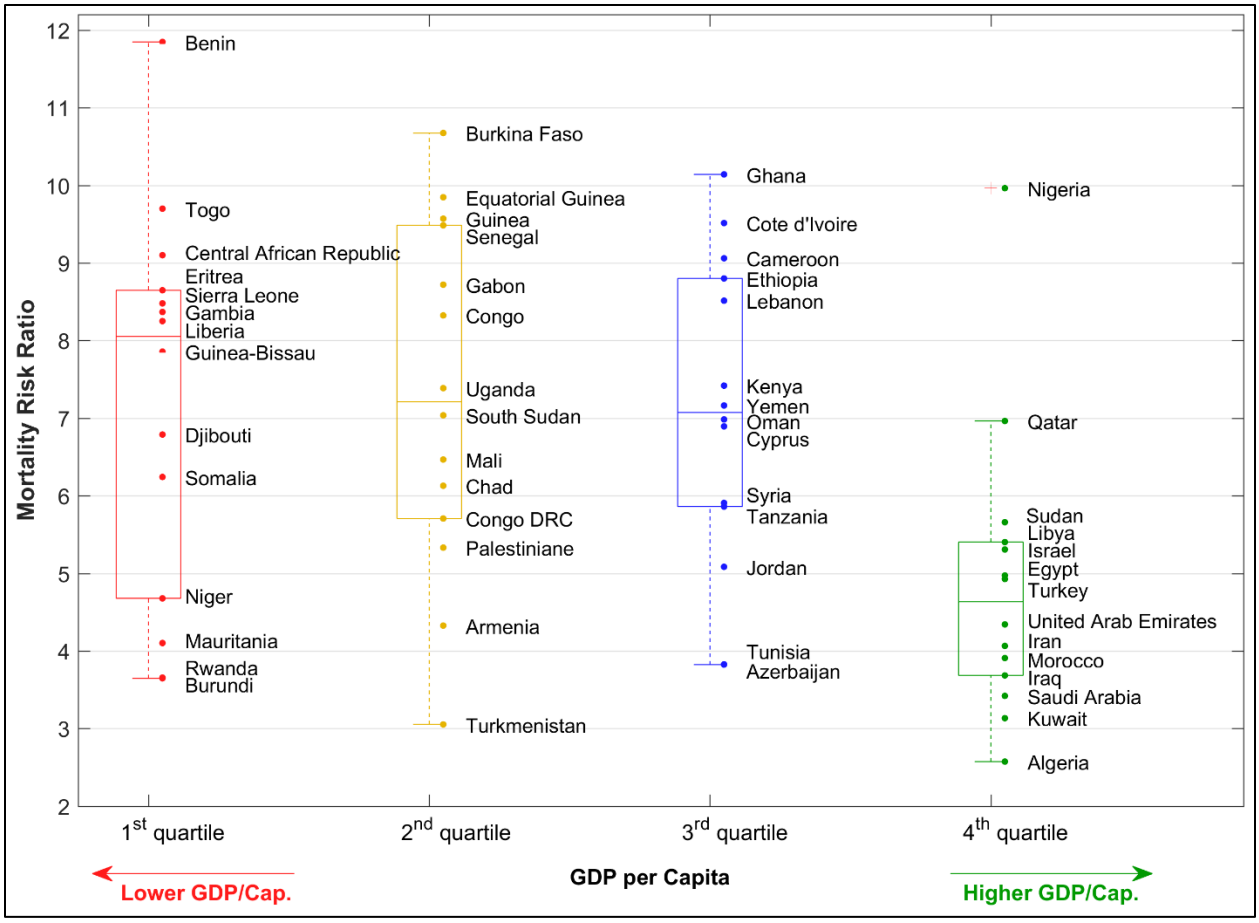

Figure S4. Same as Figure 4 in the manuscript, but for RCP4.5: Distribution of mortality risk ratio (from RCP4.5) among the 56 studied countries in the MENA region, divided into four quartiles based on their GDP (Gross Domestic Product) per capita. The line in the middle of each box represents the median mortality risk ratio in each case. The figure shows that the poorest nations (in the 1st quartile) will experience the highest mortality risk ratio, whereas wealthy countries will be least impacted by climate change (based on MRR).

3. Uncertainty characterization

This section investigates climate change uncertainties of mortality risk ratio and related influential components such as frequency of unsafe days and intensity of wet-bulb temperature rise.

3.1. Mortality risk ratio

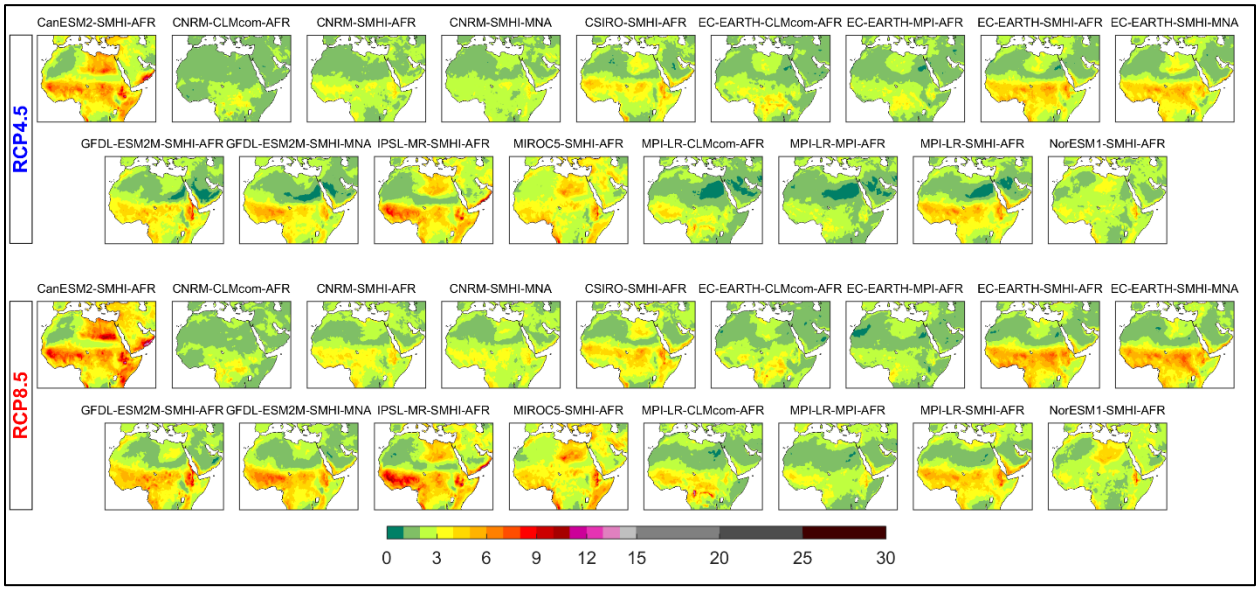

Figure S5. Mortality risk ratio for the 17 RCMs in RCP4.5 (top) and RCP8.5 (bottom) during 2010-2039.

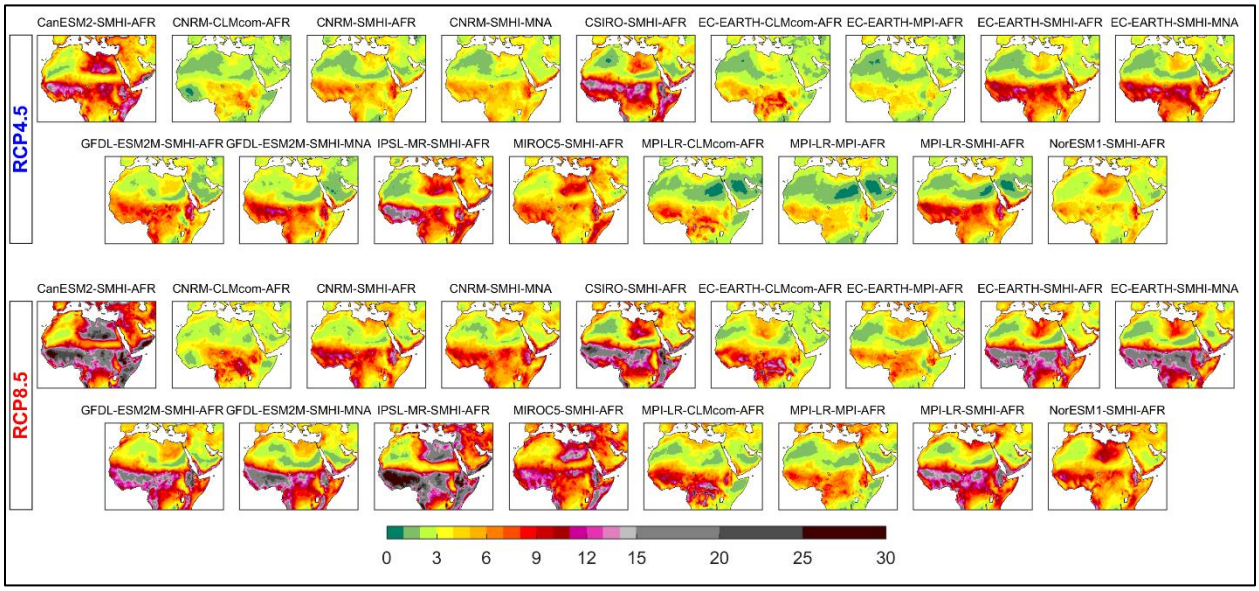

Figure S6. Mortality risk ratio for the 17 RCMs in RCP4.5 (top) and RCP8.5 (bottom) during 2040-2069.

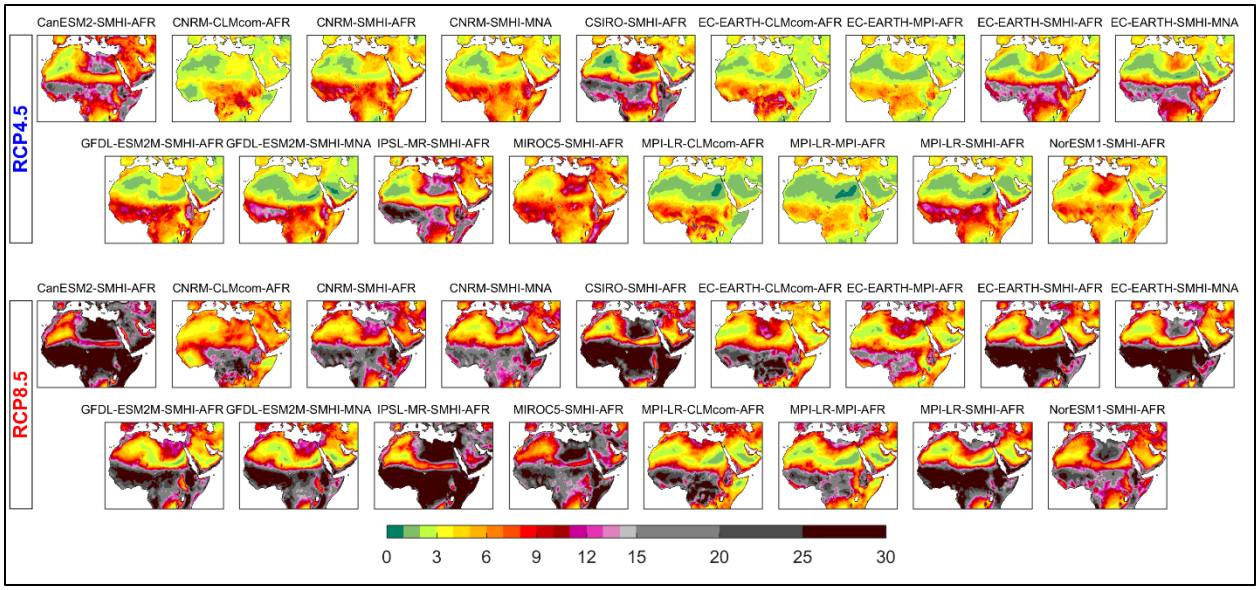

Figure S7. Mortality risk ratio for the 17 RCMs in RCP4.5 (top) and RCP8.5 (bottom) during 2070-2099.

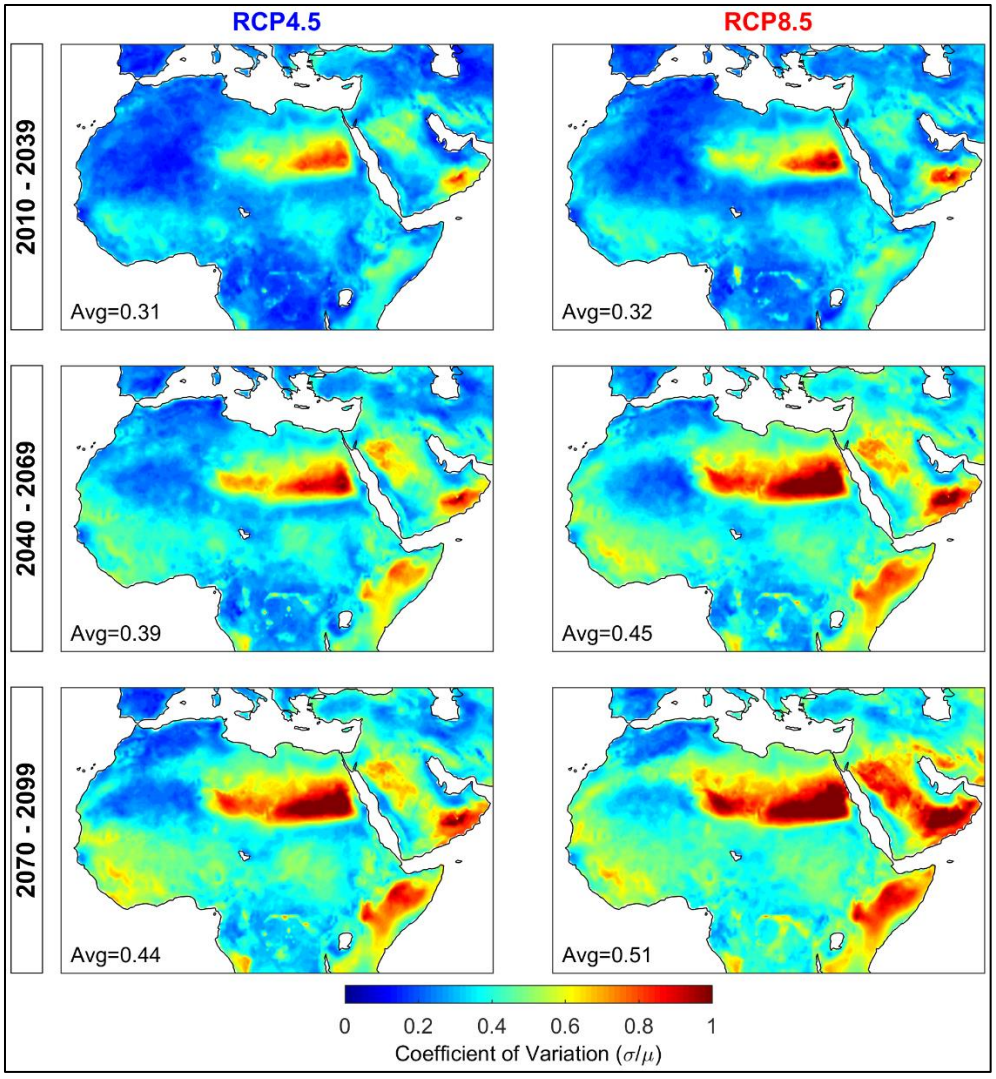

Figure S8. Coefficient of variation (CV; mean/standard deviation) of mortality risk ratio from the results of 17 RCMs. The figure shows an increasing trend over time, and indicates higher CV for RCP8.5 than RCP4.5.

3.2. Frequency (percentage) of unsafe days

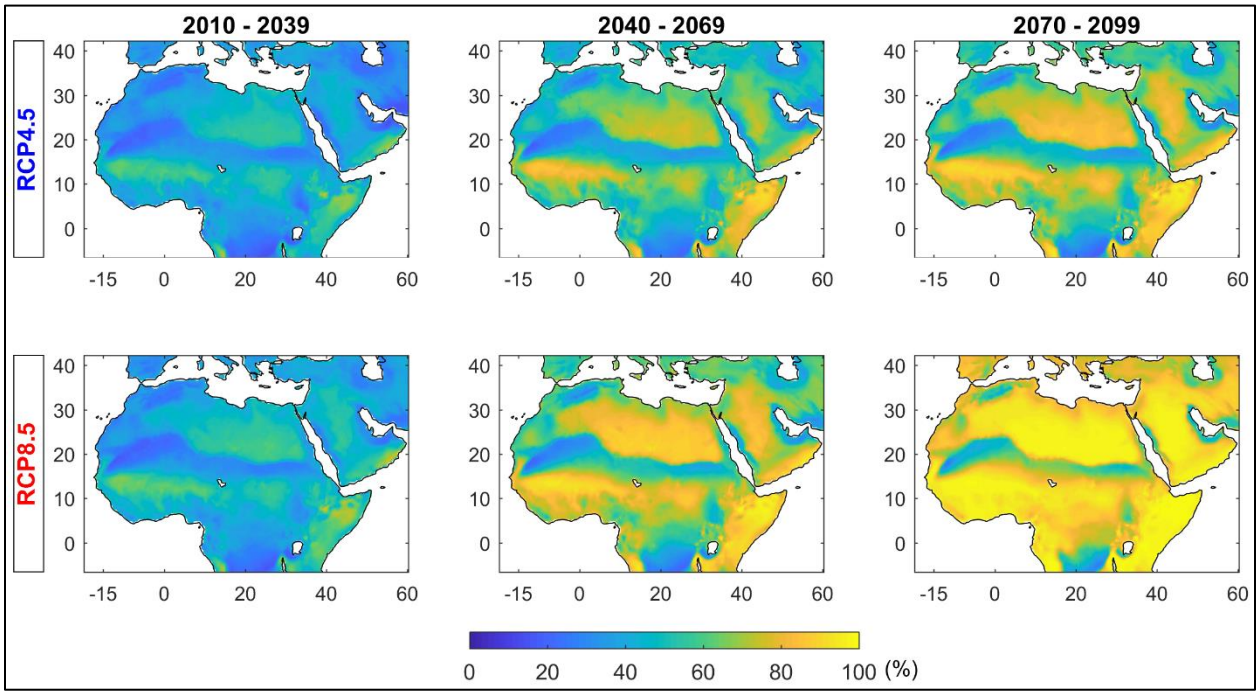

Figure S9. The frequency (percentage) of unsafe days (percentage of days with TW>Topt) during summers in each 30-year future period for RCP4.5 (top) and RCP8.5 (bottom). The figure shows the ensemble mean of 17 RCMs.

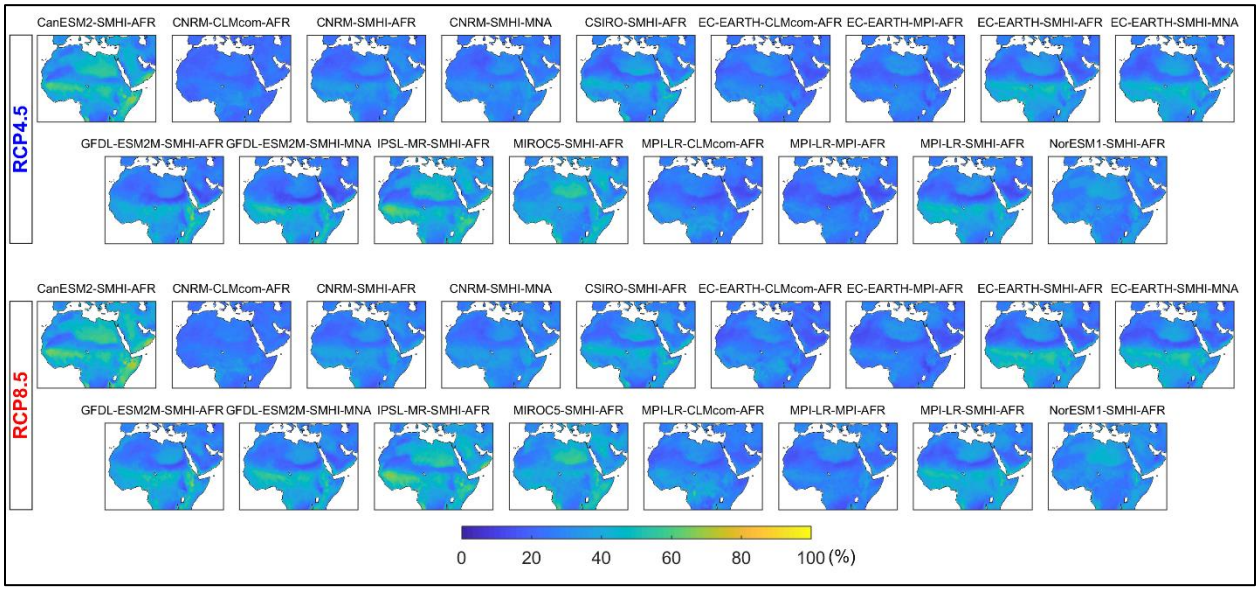

Figure S10. The frequency (percentage) of unsafe days (percentage of days with TW>Topt) during summer for each RCM in RCP4.5 (top) and RCP8.5 (bottom) during 2010-2039.

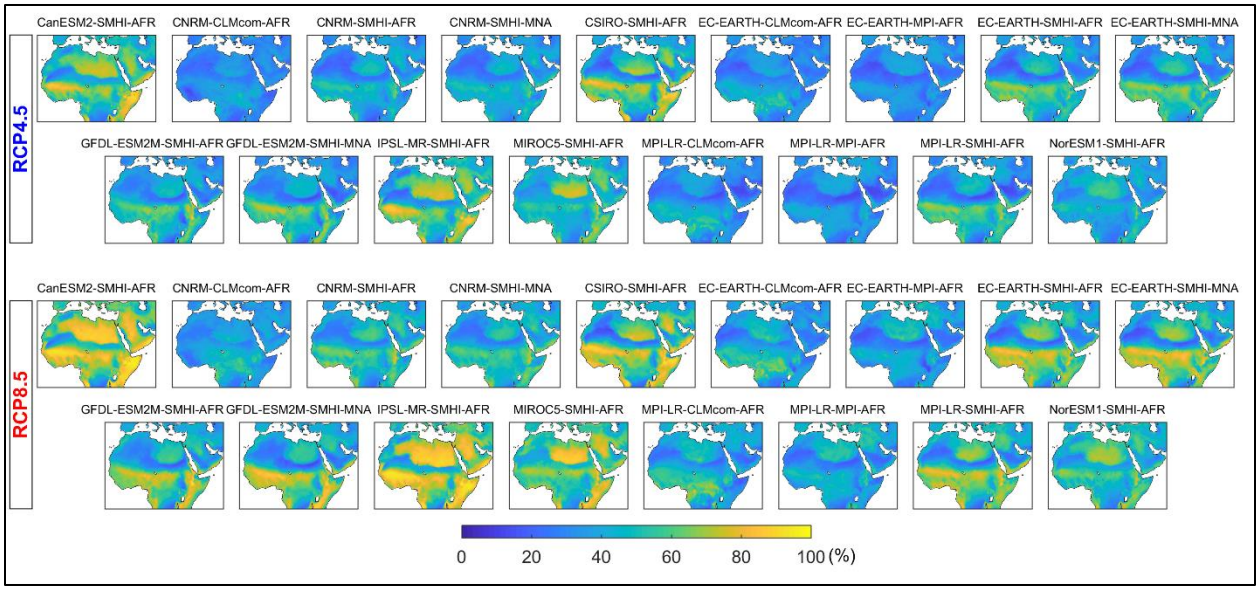

Figure S11. The frequency (percentage) of unsafe days (percentage of days with TW>Topt) during summer for each RCM in RCP4.5 (top) and RCP8.5 (bottom) during 2040-2069.

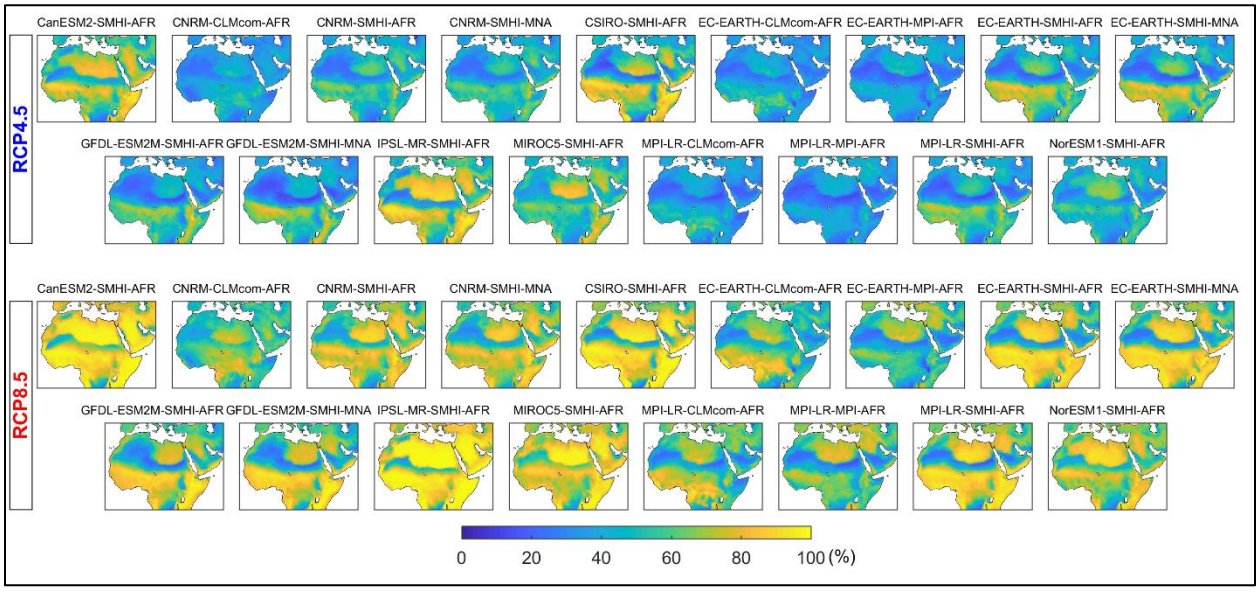

Figure S12. The frequency (percentage) of unsafe days (percentage of days with TW>Topt) during summer for each RCM in RCP4.5 (top) and RCP8.5 (bottom) during 2070-2099.

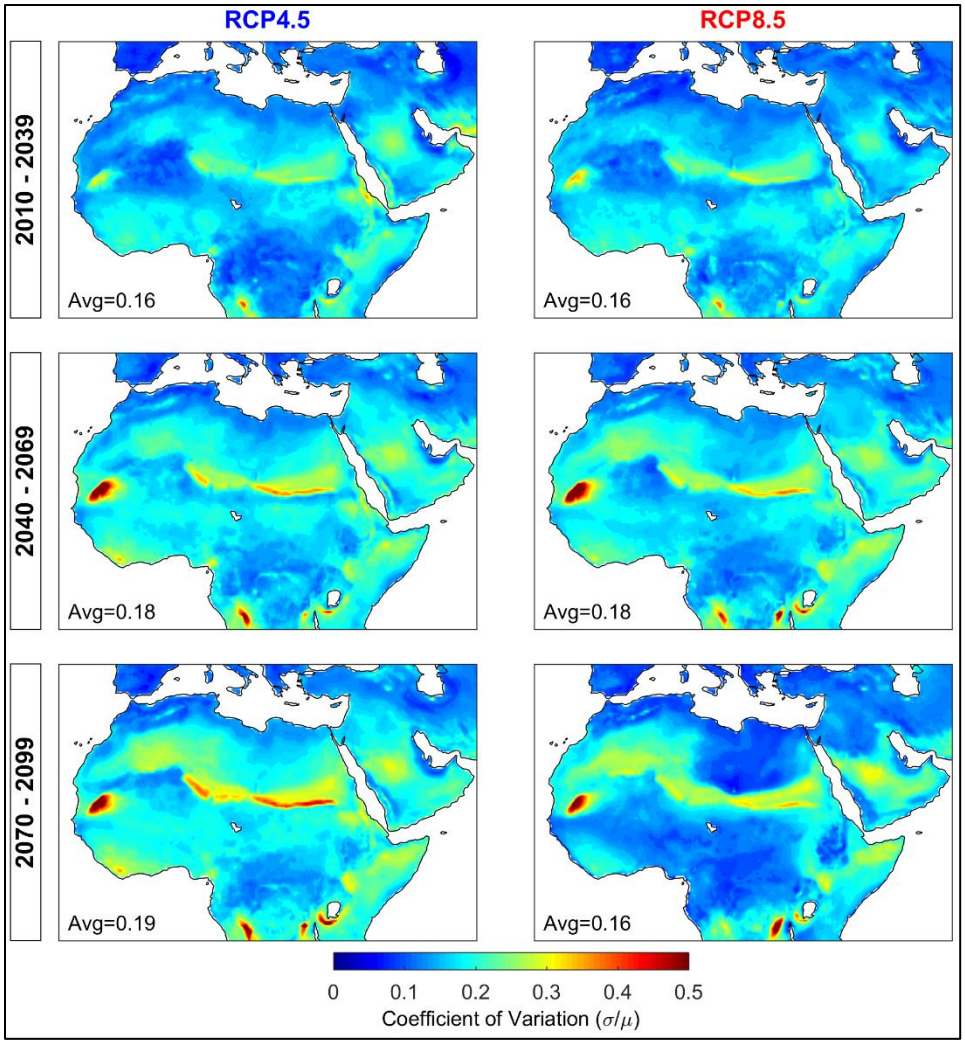

Figure S13. Coefficient of variation (CV; mean/standard deviation) of the frequency of unsafe days (percentage of days with *TW>Topt*) from the results of 17 RCMs. Unlike the results of mortality risk ratio (Figure S7), CV does not necessarily increase over time, and both concentration pathways (i.e. RCP4.5 and RCP8.5) indicate similar results. In fact, CV for frequency of unsafe days is considerably lower than that of mortality risk ratio (Figure S8) and ΔTW (Figure S18).

3.3. Intensity (ΔTW)

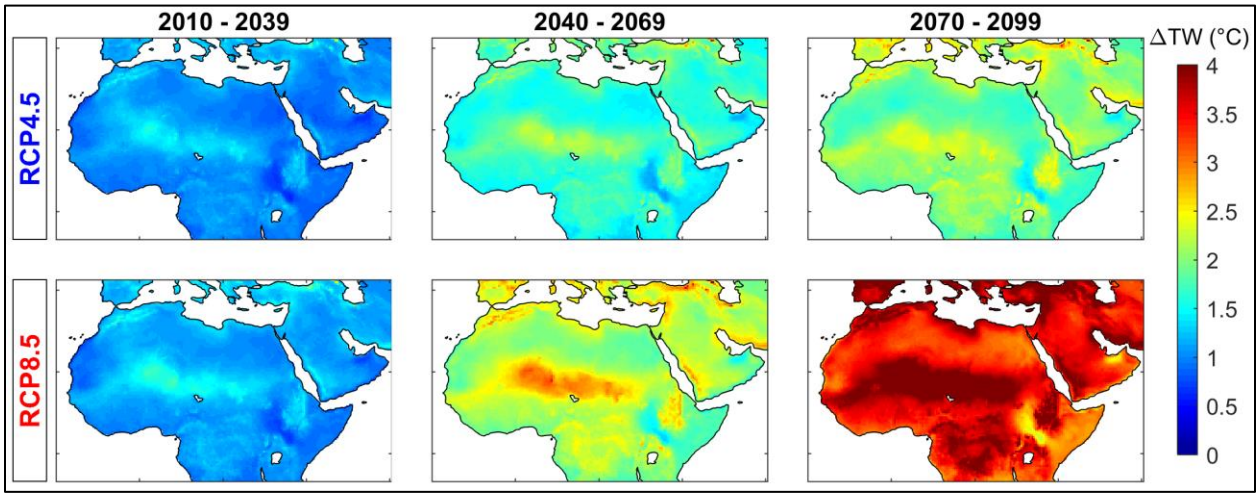

Figure S14. Mean of projected wet-bulb temperature increase (ΔTW) for 30-year future periods for RCP4.5 (top) and RCP8.5 (bottom) pathways. Mean values are calculated using data obtained from 17 RCMs.

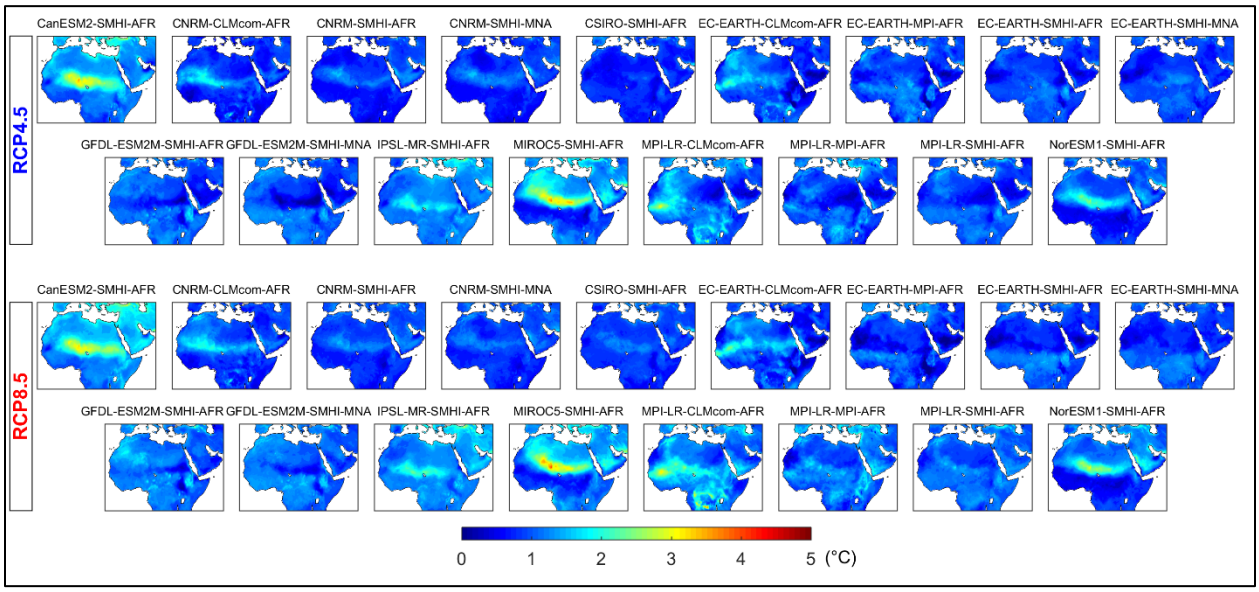

Figure S15. Projected changes of wet-bulb temperature (ΔTW) for each RCM for RCP4.5 (top) and RCP8.5 (bottom) pathways during 2010-2039.

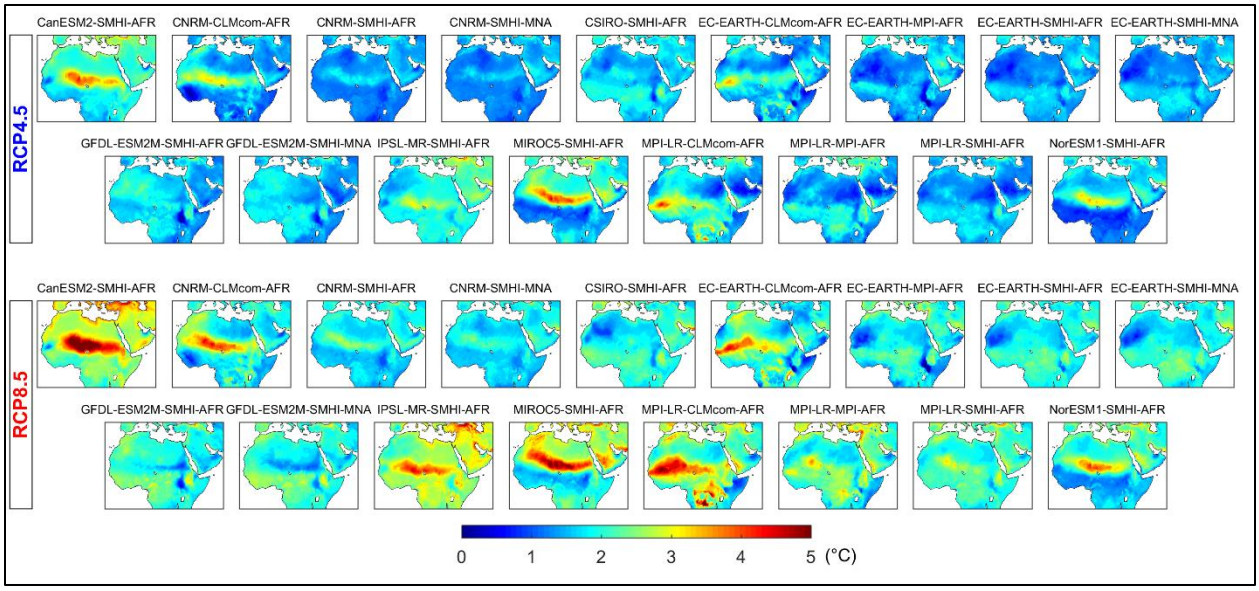

Figure S16. Projected changes of wet-bulb temperature (ΔTW) for each RCM for RCP4.5 (top) and RCP8.5 (bottom) pathways during 2040-2069.

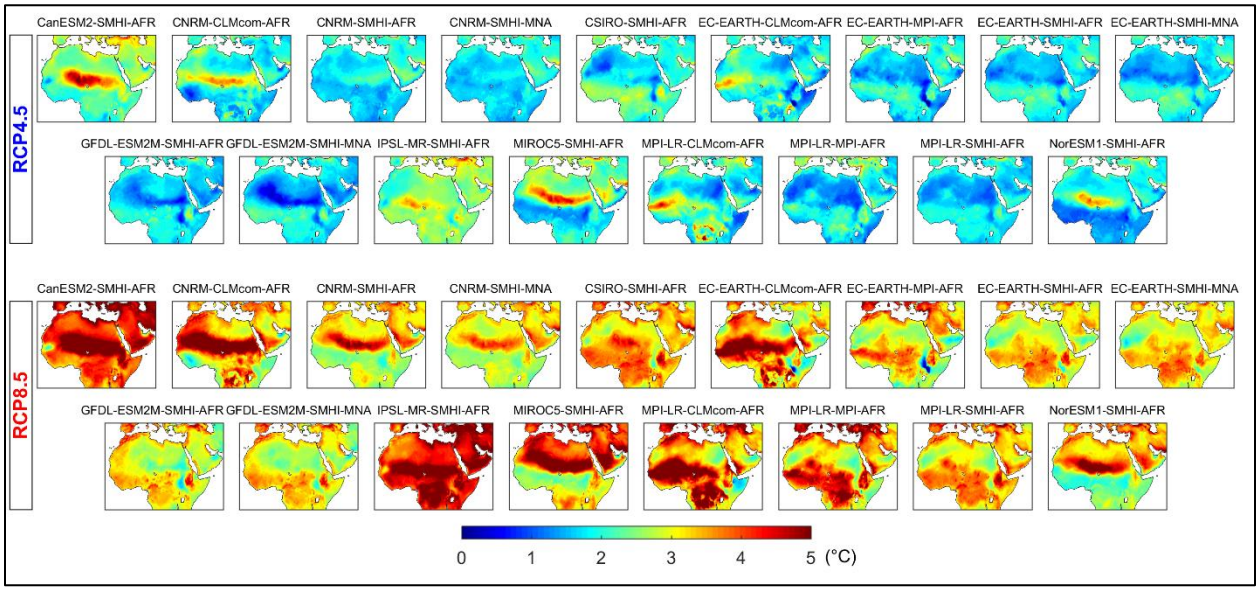

Figure S17. Projected changes of wet-bulb temperature (ΔTW) for each RCM for RCP4.5 (top) and RCP8.5 (bottom) pathways during 2070-2099.

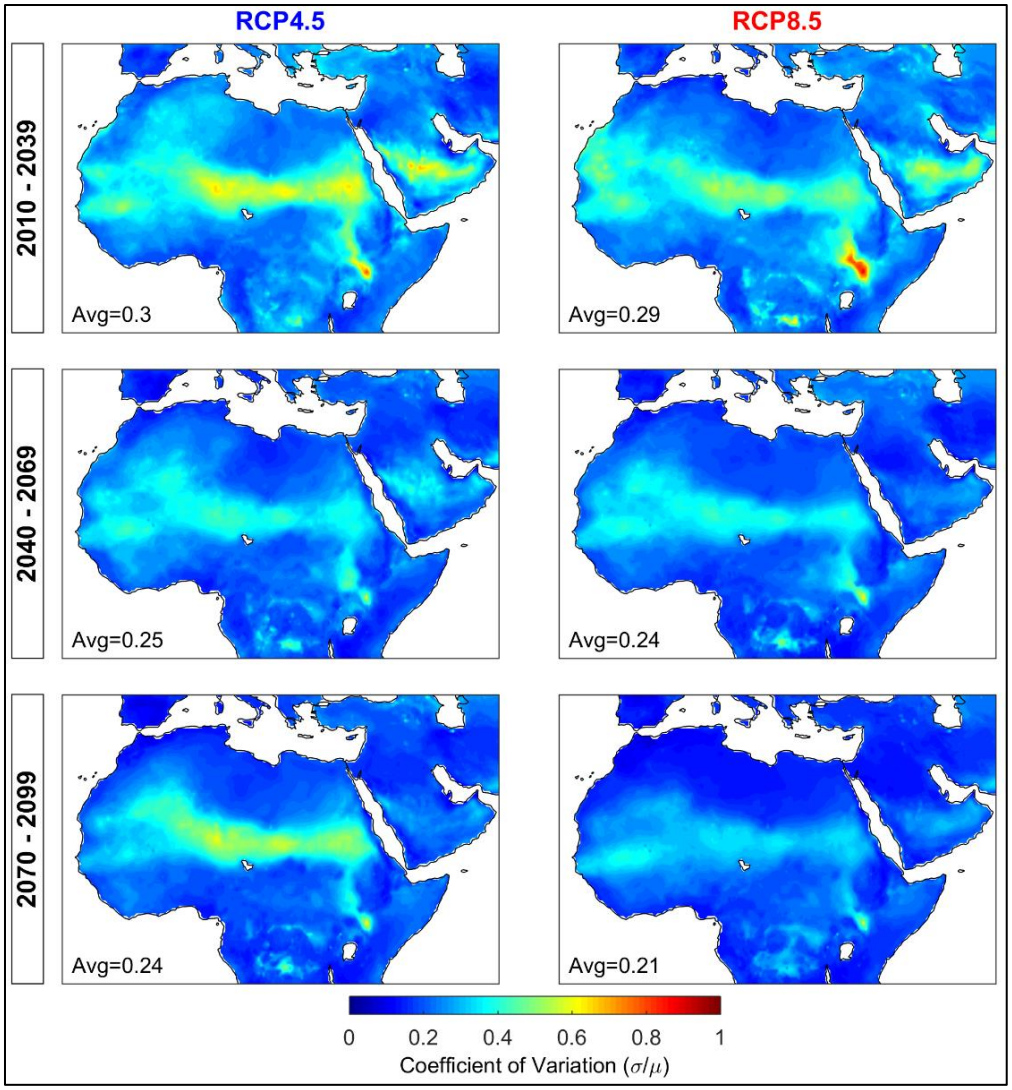

Figure S18. Coefficient of variation (CV; mean/standard deviation) of wet-bulb temperature changes (ΔTW) from the results of 17 RCMs. The figure shows a decreasing trend over time, and indicates a higher CV for RCP4.5 than RCP8.5 (contrary to the patterns of mortality risk ratio).

4. Synthesis for 10 major cities

Here, we investigate the impacts of climate change on mortality risk ratio and related components such as intensity of unsafe temperatures (ΔTW) and frequency of unsafe days, for 10 major cities in the study area. First, the temporal changes of each variable are presented during 2006-2100. Then, the changes of mortality risk ratio across the three selected future periods are assessed for each city by investigating probability distribution functions. At last, the time of emergence for three different levels of mortality risk ratio is studied for each city. Table S2 provides a summary of the 10 selected cities, their current population, and the corresponding mean mortality risk ratio for each future period and scenario. All 10 selected cities have high population and the majority of them are tourist destinations, meaning that heat stress induced mortality are expected to have significant impact, both economically and socially.

Table S2. Future mortality risk in 10 major cities of MENA.

No.	City	Lat	Lon	Current Population (millions)	Mean Mortality Risk Ratio					
					RCP4.5			RCP8.5		
					2010-2039	2040-2069	2070-2099	2010-2039	2040-2069	2070-2099
1	Addis Ababa, Ethiopia	8.8	38.72	4.6	3.6	7.4	11.3	4.0	12.0	30.5
2	Barcelona, Spain	41.36	2.2	5.4	2.4	4.7	6.4	2.6	6.6	16.7
3	Cairo, Egypt	29.92	31.24	20	2.0	3.5	4.5	2.3	5.2	12.2
4	Doha, Qatar	25.08	51.48	1.4	2.7	4.6	6.4	2.9	7.1	15.7
5	Dubai, UAE	25.08	55.44	5.6	2.2	4.1	5.4	2.6	5.7	12.8
6	Istanbul, Turkey	29.04	40.92	14.7	1.3	2.0	2.5	1.4	2.9	5.6
7	Lagos, Nigeria	6.6	3.08	21	3.3	7.0	10.3	3.4	10.9	26.2
8	Mecca, Saudi Arabia	21.56	39.6	1.7	2.1	3.5	4.4	2.2	5.1	10.4
9	Rome, Italy	41.8	12.76	4.4	2.4	4.6	6.4	2.9	6.6	16.0
10	Tehran, Iran	35.64	51.48	15	2.0	3.0	4.0	2.1	4.5	8.5

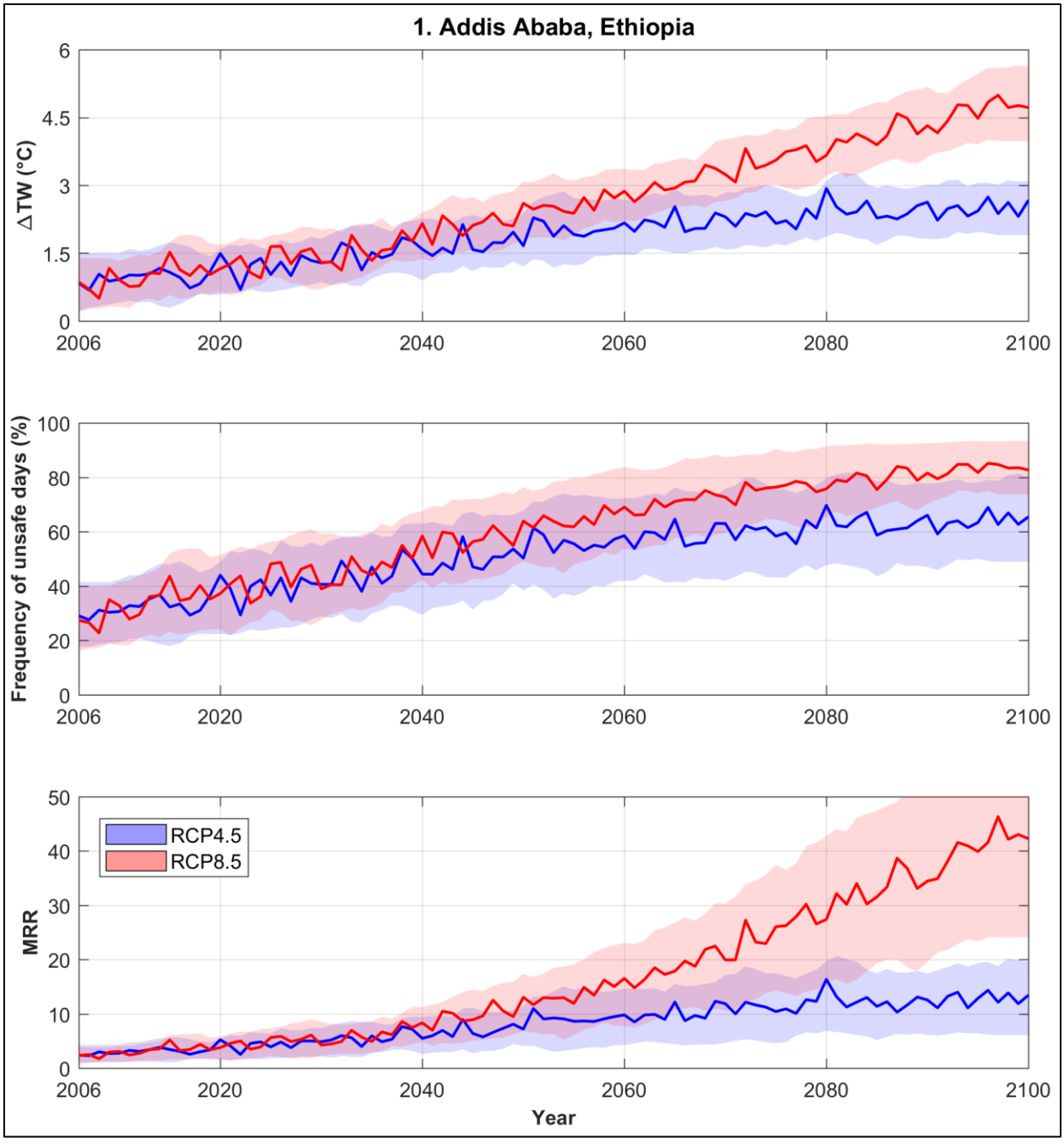

Figure S19. Temporal variation of ΔTW (top), frequency of unsafe days (middle), and mortality risk ratio (MRR; bottom) in future during 2006-2100 for Addis Ababa, Ethiopia. The bold line represents the ensemble mean of 17 RCMs and the shaded area indicates ±1 standard deviation.

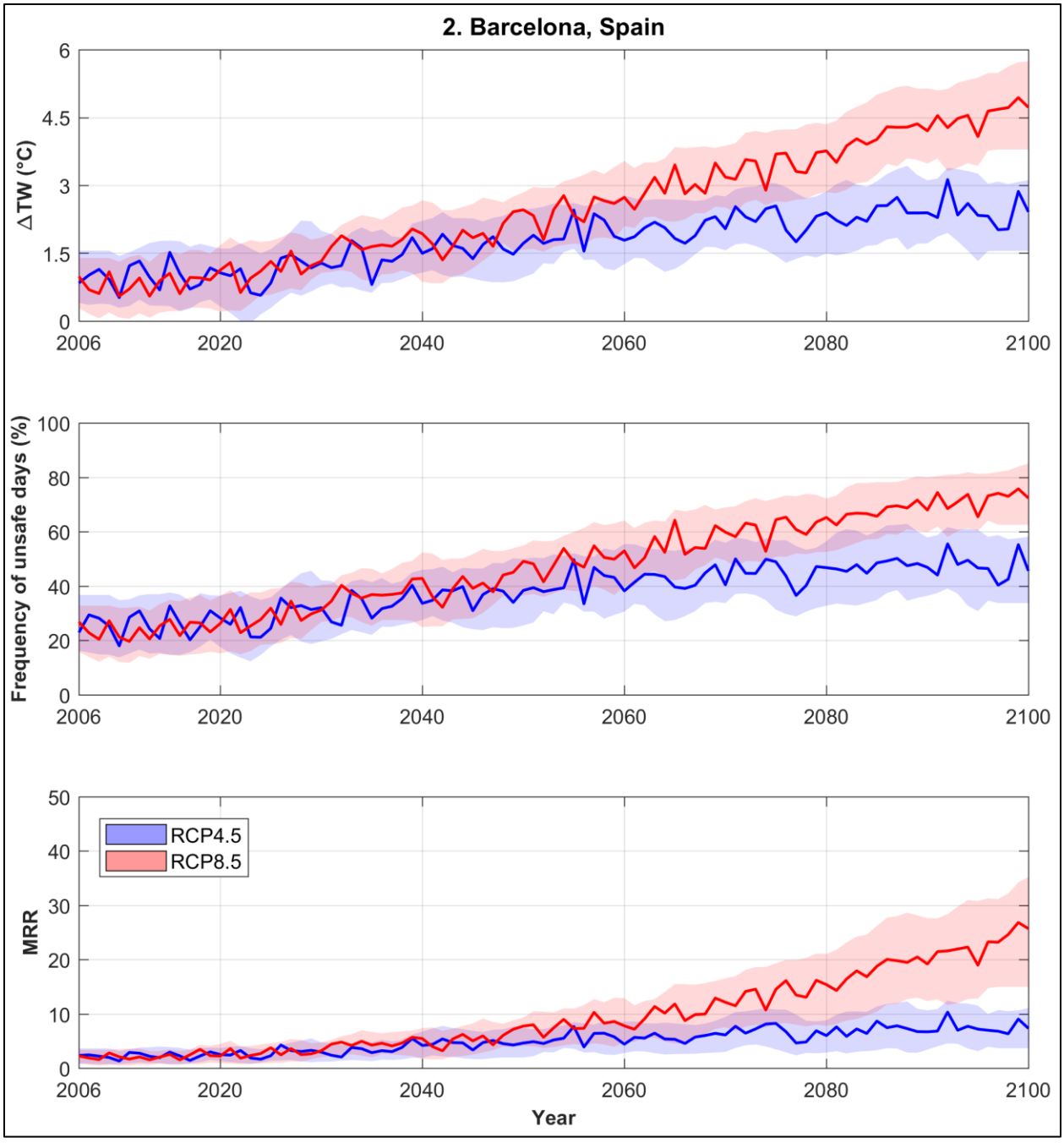

Figure S20. Temporal variation of ΔTW (top), frequency of unsafe days (middle), and mortality risk ratio (MRR; bottom) in future during 2006-2100 for Barcelona, Spain. The bold line represents the ensemble mean of 17 RCMs and the shaded area indicates ±1 standard deviation.

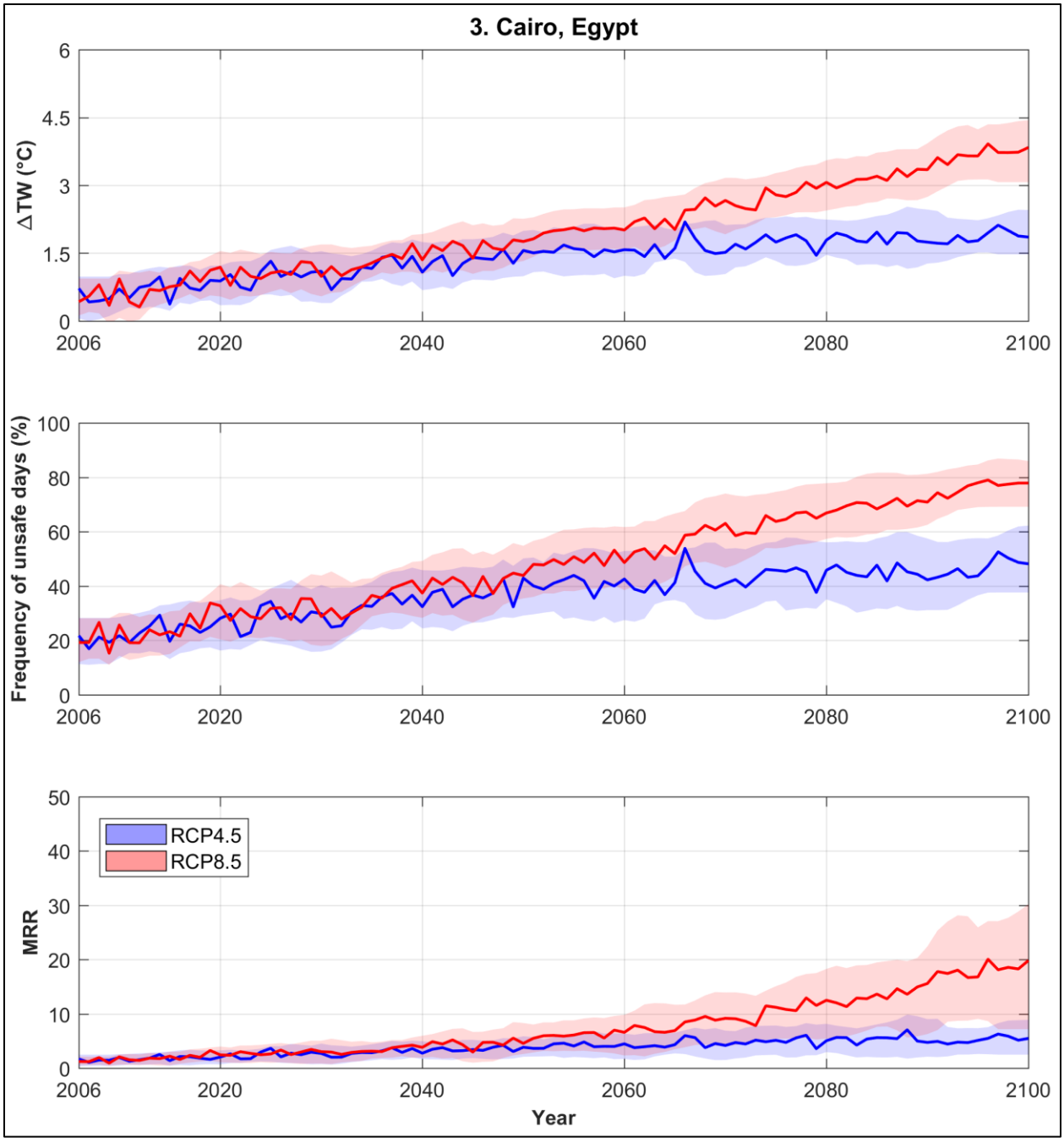

Figure S21. Temporal variation of ΔTW (top), frequency of unsafe days (middle), and mortality risk ratio (MRR; bottom) in future during 2006-2100 for Cairo, Egypt. The bold line represents the ensemble mean of 17 RCMs and the shaded area indicates ±1 standard deviation.

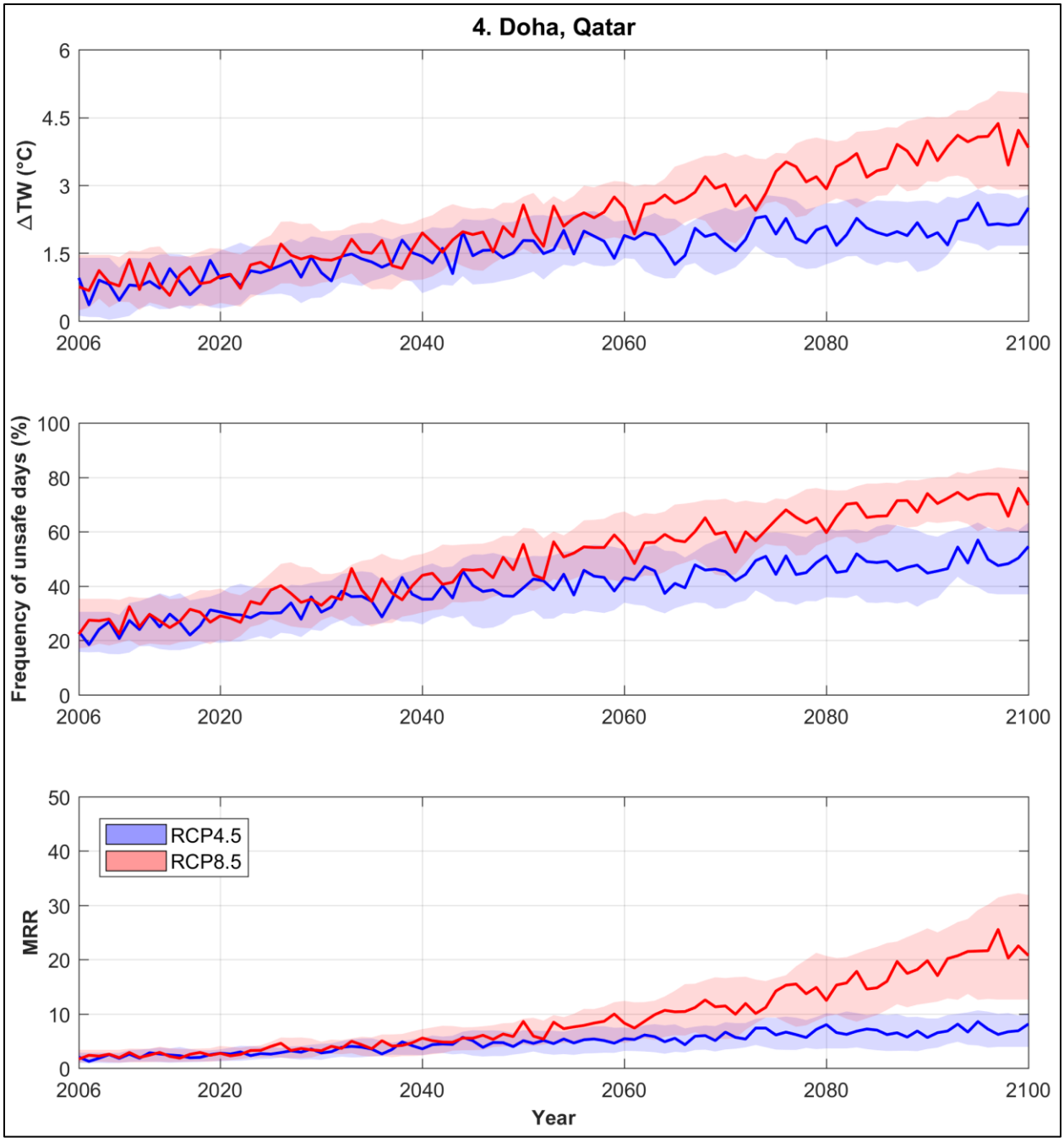

Figure S22. Temporal variation of ΔTW (top), frequency of unsafe days (middle), and mortality risk ratio (MRR; bottom) in future during 2006-2100 for Doha, Qatar. The bold line represents the ensemble mean of 17 RCMs and the shaded area indicates ±1 standard deviation.

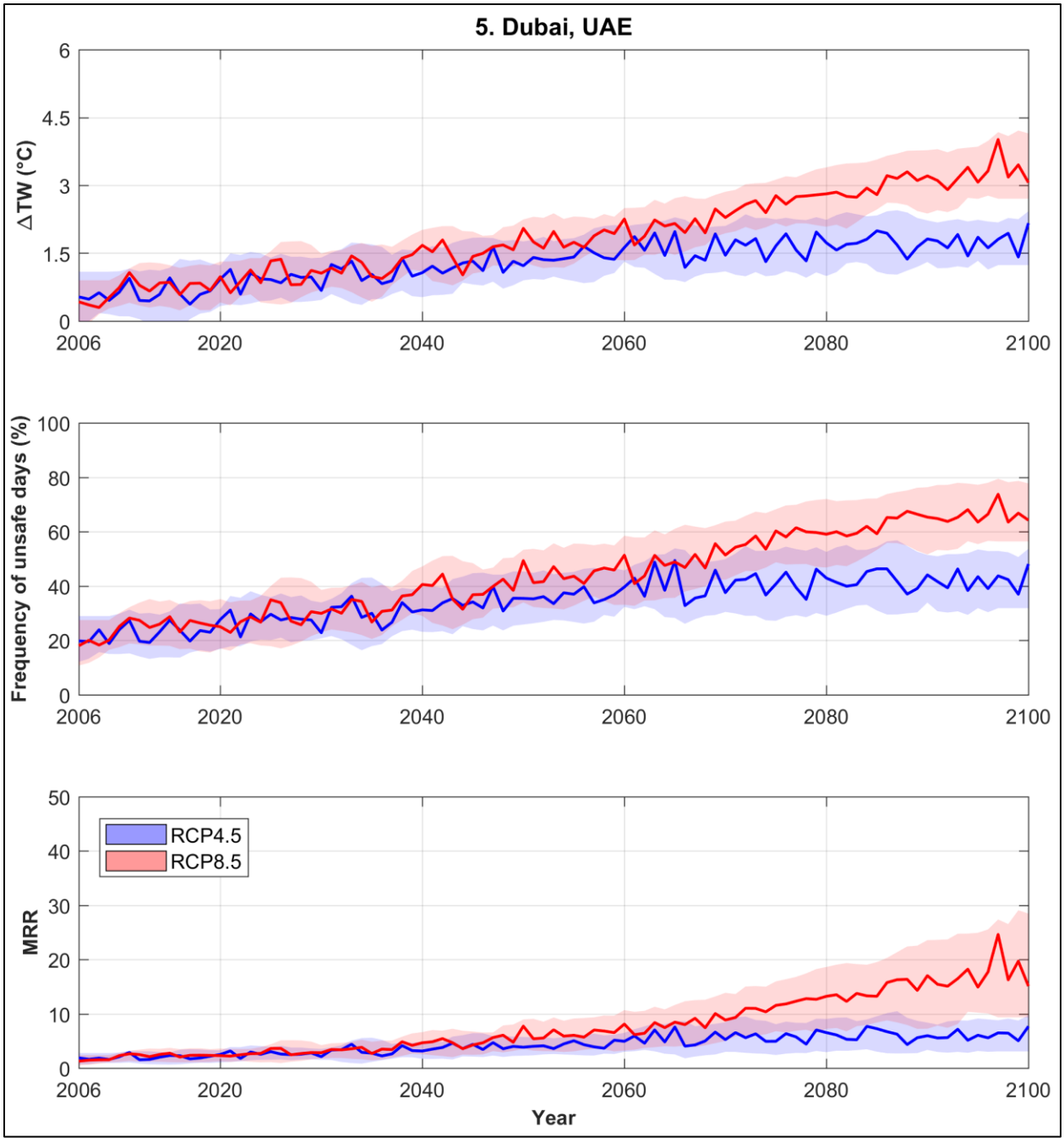

Figure S23. Temporal variation of ΔTW (top), frequency of unsafe days (middle), and mortality risk ratio (MRR; bottom) in future during 2006-2100 for Dubai, United Arab Emirates. The bold line represents the ensemble mean of 17 RCMs and the shaded area indicates ±1 standard deviation.

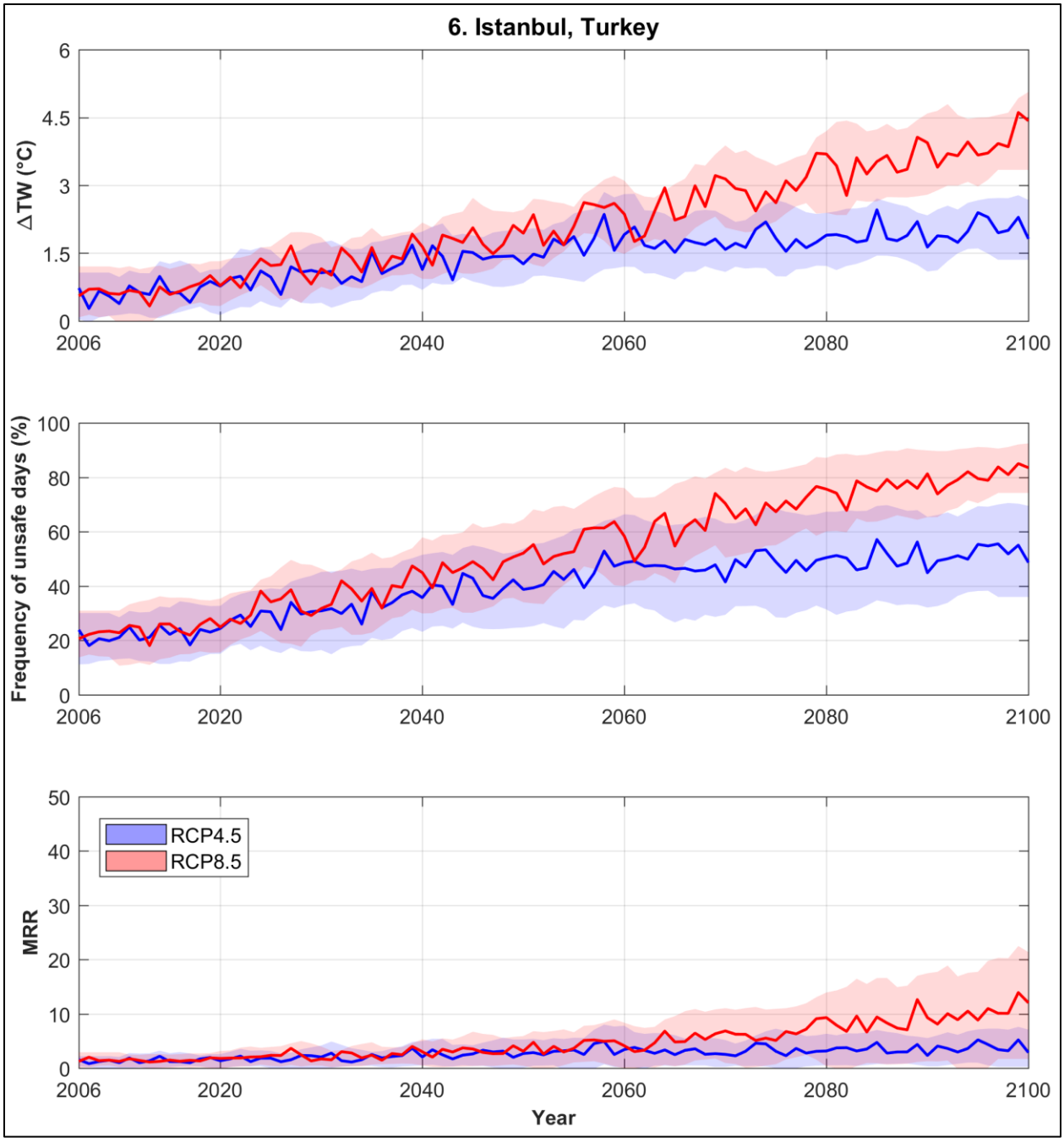

Figure S24. Temporal variation of ΔTW (top), frequency of unsafe days (middle), and mortality risk ratio (MRR; bottom) in future during 2006-2100 for Istanbul, Turkey. The bold line represents the ensemble mean of 17 RCMs and the shaded area indicates ±1 standard deviation.

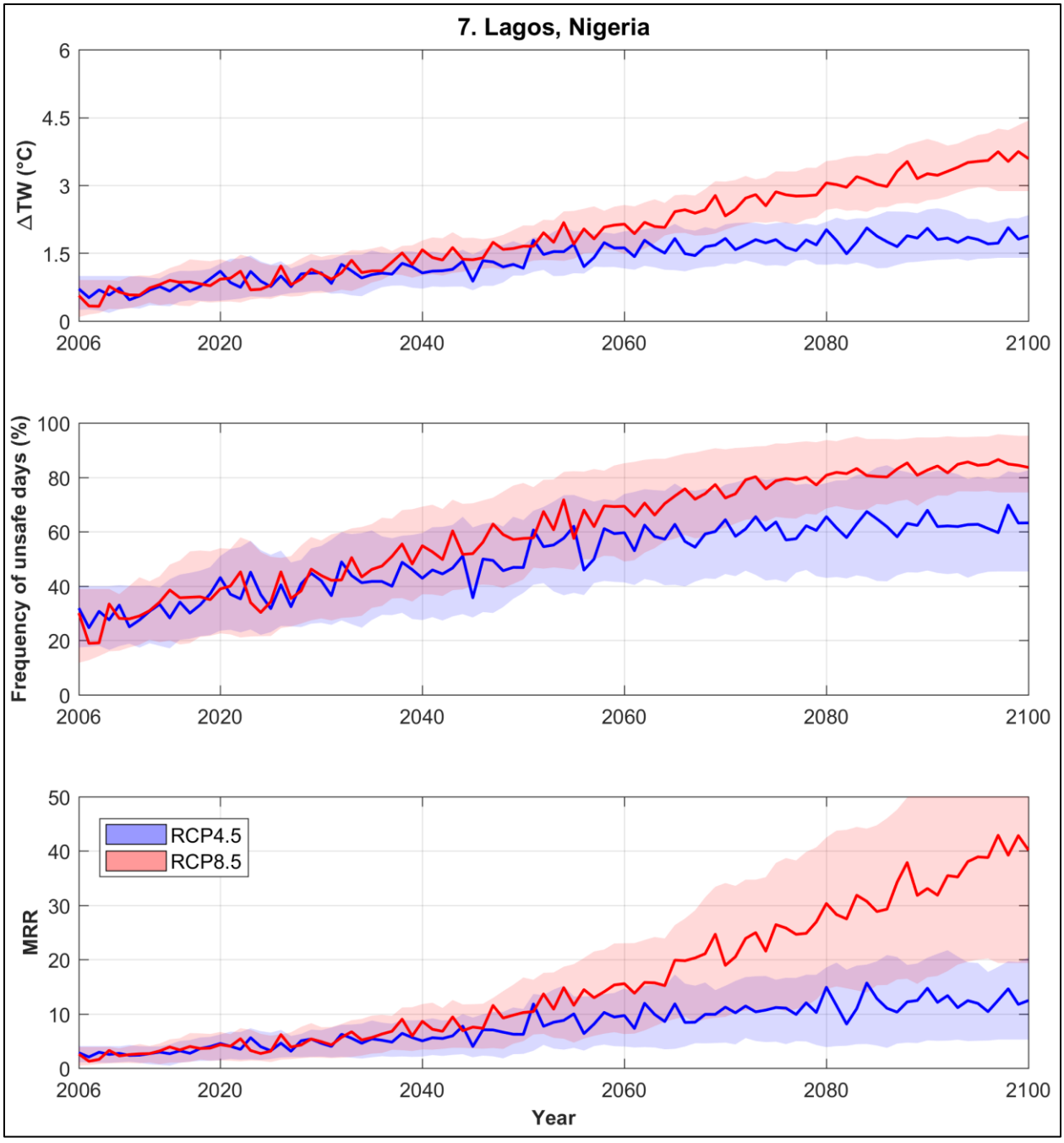

Figure S25. Temporal variation of ΔTW (top), frequency of unsafe days (middle), and mortality risk ratio (MRR; bottom) in future during 2006-2100 for Lagos, Nigeria. The bold line represents the ensemble mean of 17 RCMs and the shaded area indicates ±1 standard deviation.

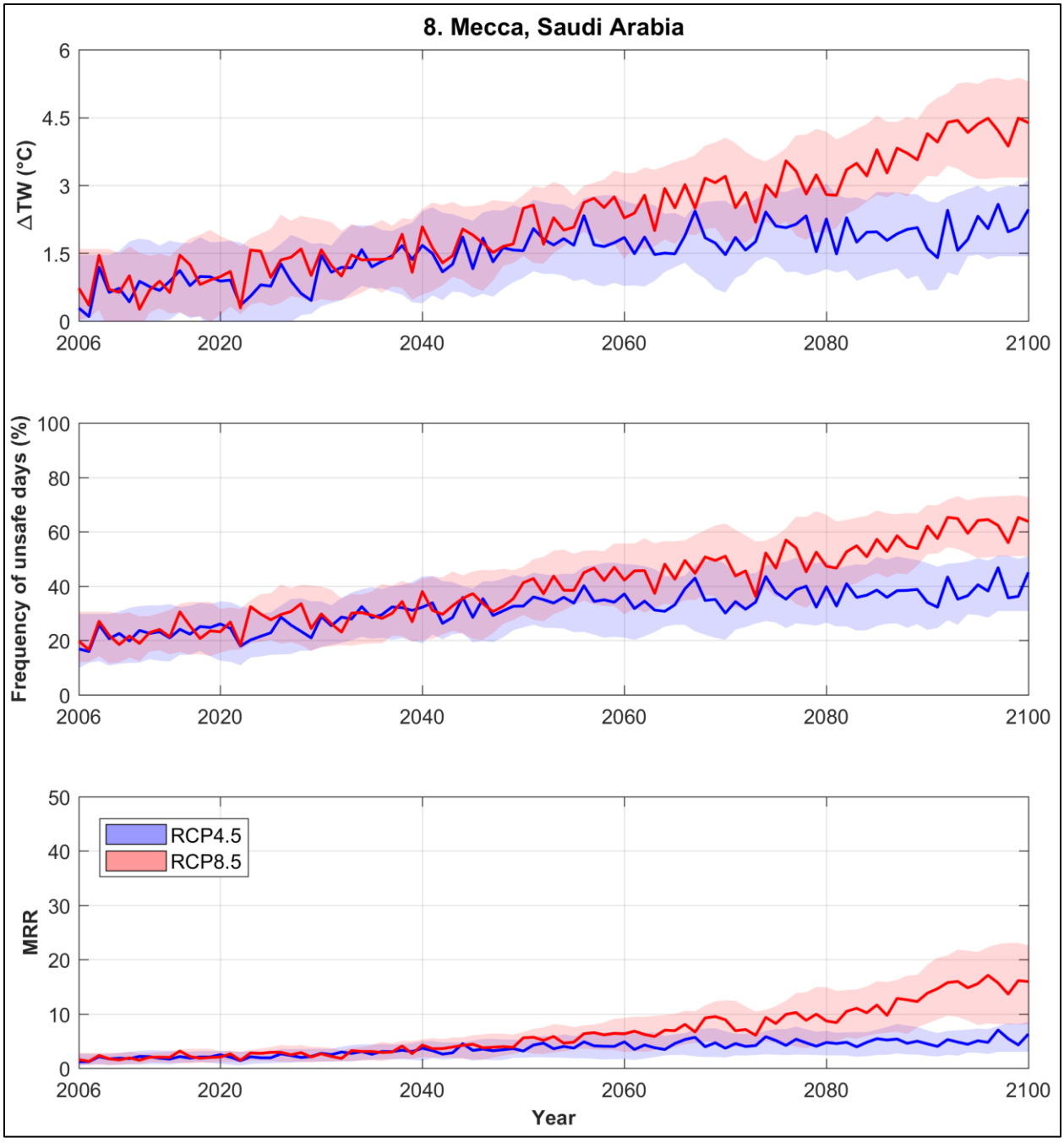

Figure S26. Temporal variation of ΔTW (top), frequency of unsafe days (middle), and mortality risk ratio (MRR; bottom) in future during 2006-2100 for Mecca, Saudi Arabia. The bold line represents the ensemble mean of 17 RCMs and the shaded area indicates ±1 standard deviation.

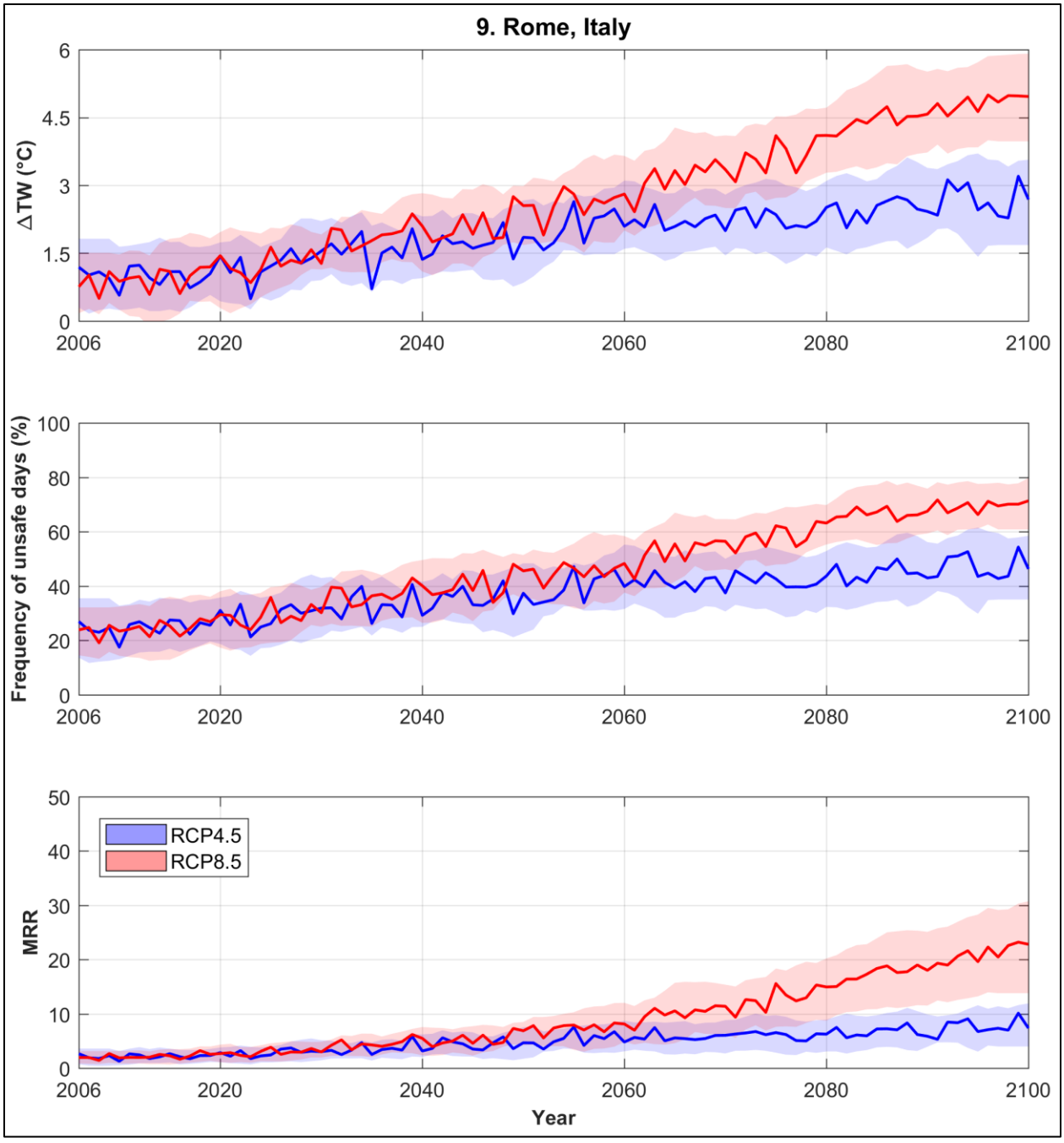

Figure S27. Temporal variation of ΔTW (top), frequency of unsafe days (middle), and mortality risk ratio (MRR; bottom) in future during 2006-2100 for Rome, Italy. The bold line represents the ensemble mean of 17 RCMs and the shaded area indicates ±1 standard deviation.

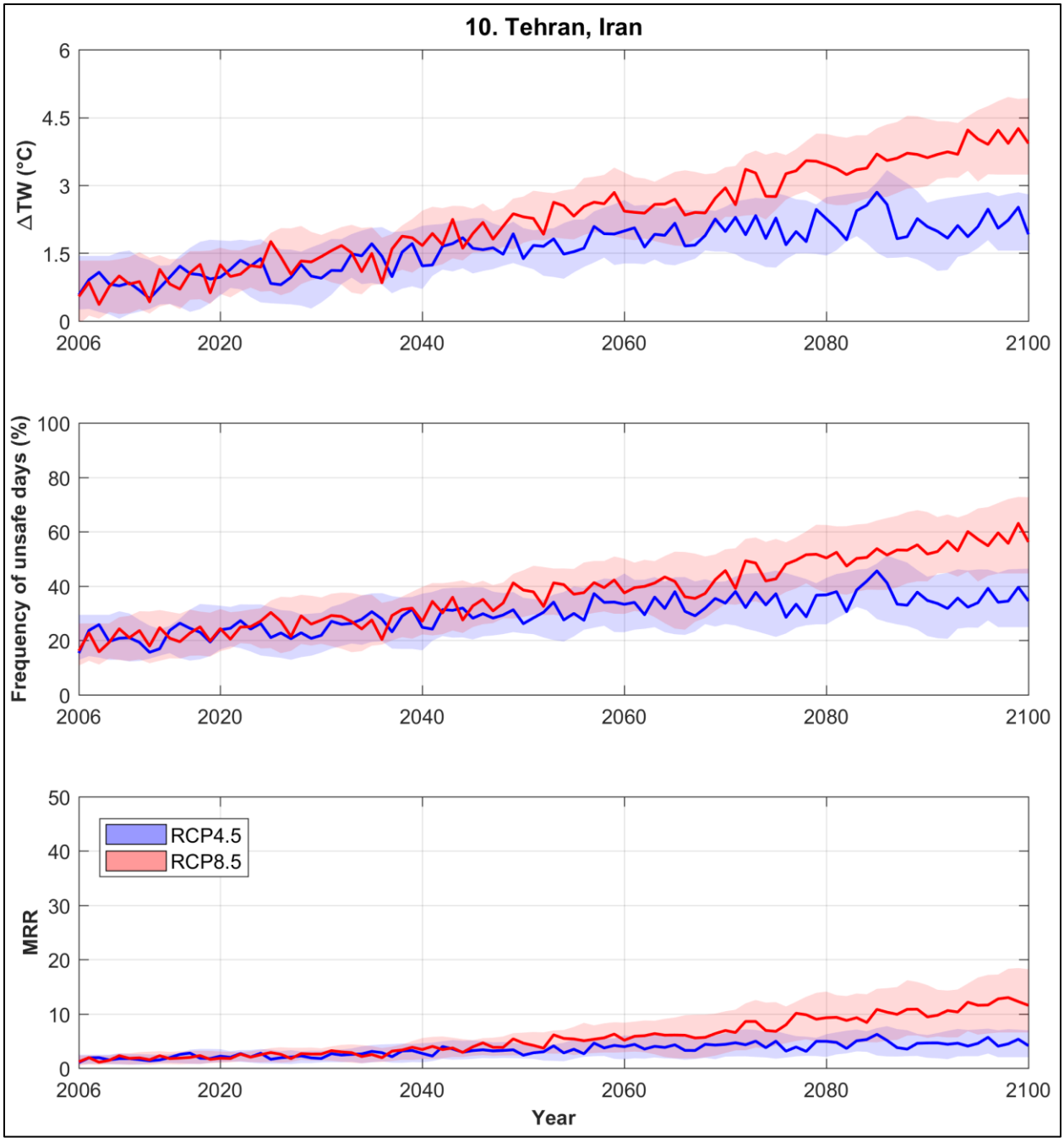

Figure S28. Temporal variation of ΔTW (top), frequency of unsafe days (middle), and mortality risk ratio (MRR; bottom) in future during 2006-2100 for Tehran, Iran. The bold line represents the ensemble mean of 17 RCMs and the shaded area indicates ±1 standard deviation.

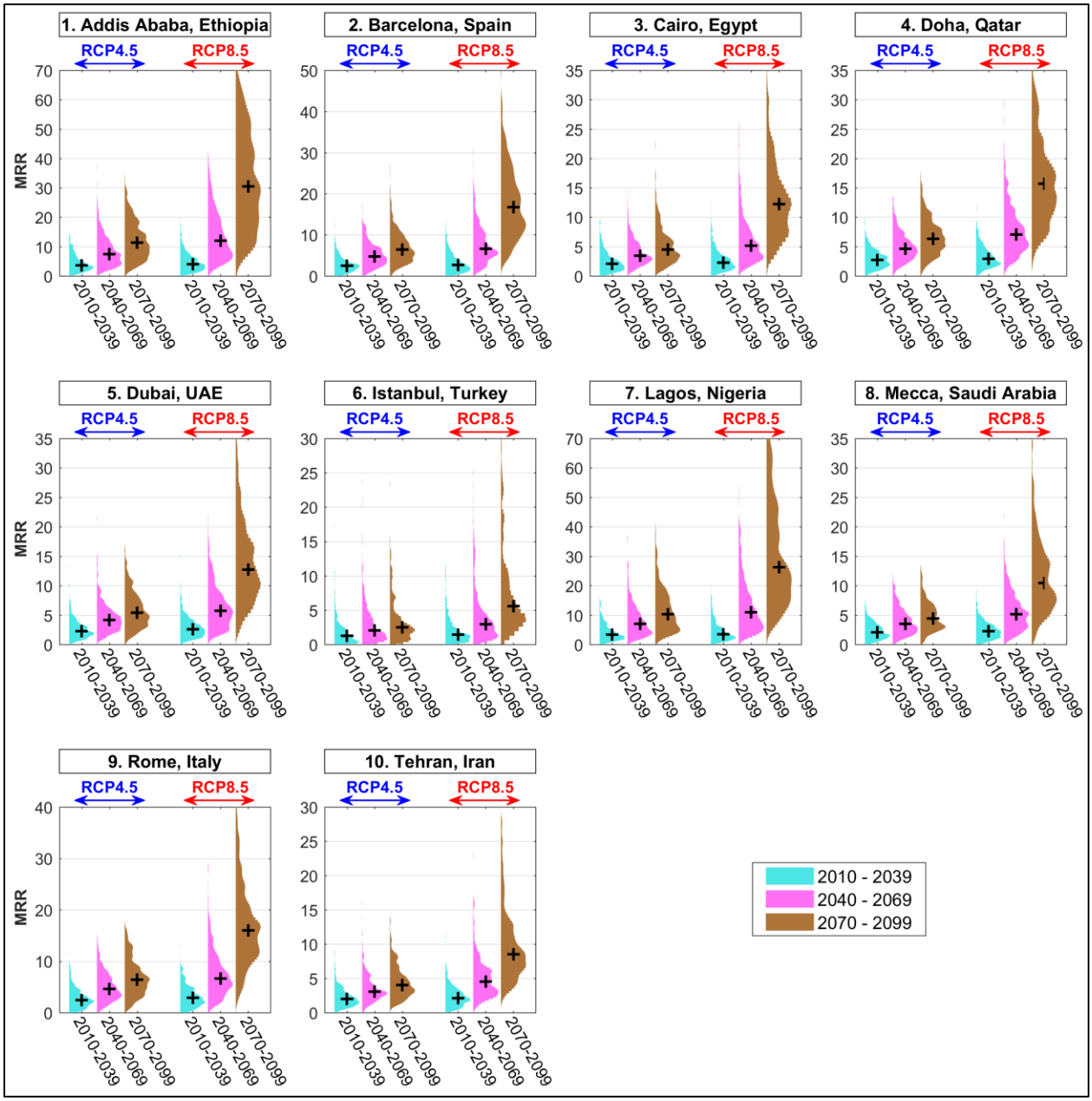

Figure S29. Violin plots presenting the distribution of mortality risk ratio (MRR) in each 30-year future periods (each specified using different colors) for the 10 major cities. Each plot is generated from 30 years of data from 17 RCMs, and the '+' sign represents the median of each plot.

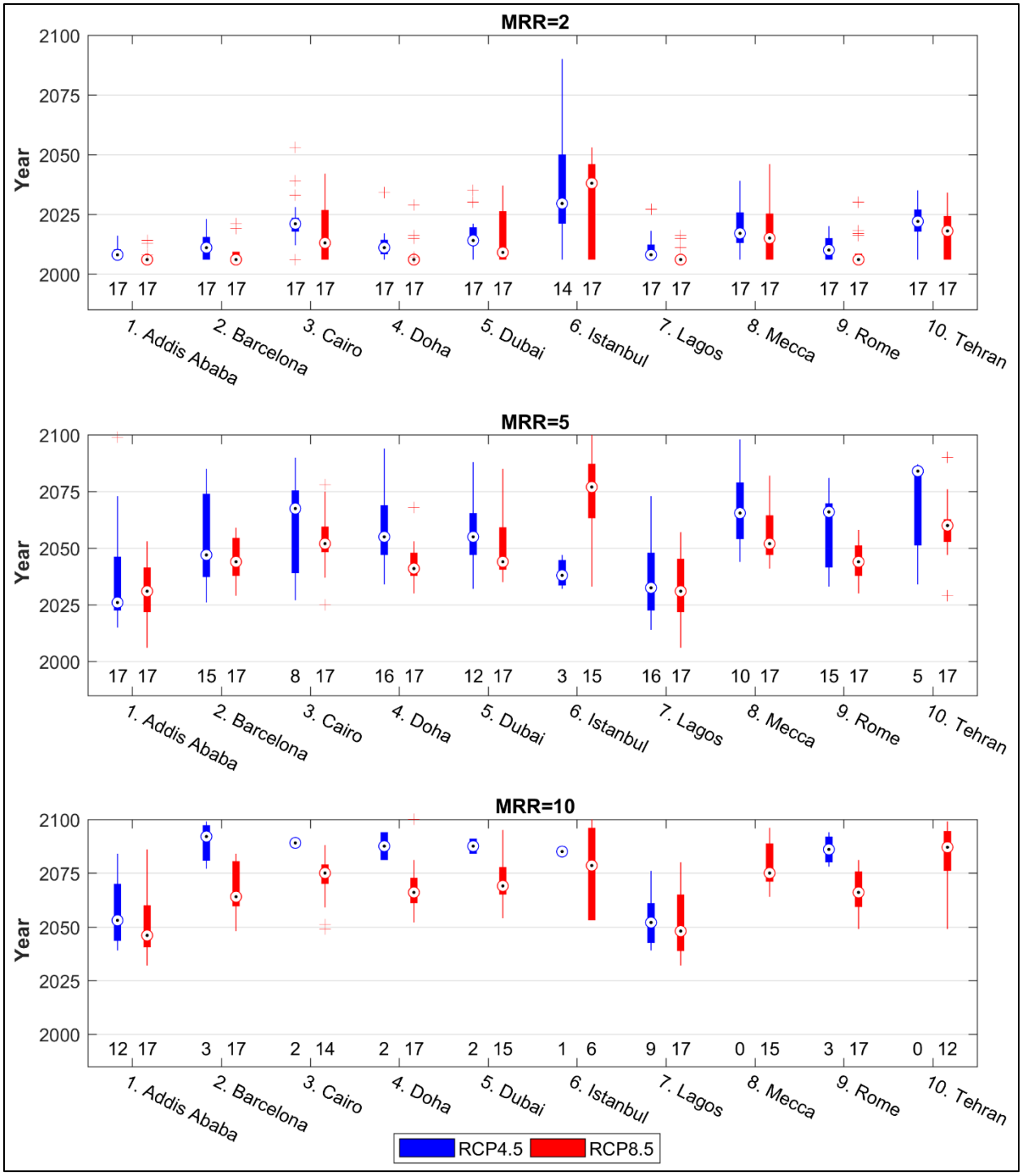

Figure S30. The time for MRR to become 2-fold (top), 5-fold (middle), and 10-fold (bottom) for each of the 10 major cities (presented on x-axis) in RCP4.5 (shown in blue) and RCP8.5 (shown in red). Boxplots show the variation of RCMs and the center dot identifies the ensemble mean. For each case, the number of RCMs for which MRR reaches the threshold value (2, 5 and 10) is indicated on the x-axis.

5. References

Ahmadalipour A, Moradkhani H (2018) Escalating heat-stress mortality risk due to global warming in the Middle East and North Africa (MENA). Environ Int 117:215–225. doi: https://doi.org/10.1016/j.envint.2018.05.014

Coffel ED, Horton RM, de Sherbinin A (2017) Temperature and humidity based projections of a rapid rise in global heat stress exposure during the 21st century. Environ Res Lett 13:14001

Honda Y, Kondo M, McGregor G, et al (2014) Heat-related mortality risk model for climate change impact projection. Environ Health Prev Med 19:56–63

Im E-S, Kang S, Eltahir EAB (2018) Projections of rising heat stress over the western Maritime Continent from dynamically downscaled climate simulations. Glob Planet Change

Pal JS, Eltahir EAB (2016) Future temperature in southwest Asia projected to exceed a threshold for human adaptability. Nat Clim Chang 6:197–200

Stull R (2011) Wet-bulb temperature from relative humidity and air temperature. J Appl Meteorol Climatol 50:2267–2269

WHO (2014) Quantitative risk assessment of the effects of climate change on selected causes of death, 2030s and 2050s. World Health Organization